# Spectroscopic Studies on the Metal–Insulator Transition Mechanism in Correlated Materials

*So Yeun Kim, Min-Cheol Lee, Garam Han, Marie Kratochvilova, Seokhwan Yun, Soon Jae Moon, Changhee Sohn, Je-Geun Park, Changyoung Kim,* and Tae Won Noh*

The metal–insulator transition (MIT) in correlated materials is a novel phenomenon that accompanies a large change in resistivity, often many orders of magnitude. It is important in its own right but its switching behavior in resistivity can be useful for device applications. From the material physics point of view, the starting point of the research on the MIT should be to understand the microscopic mechanism. Here, an overview of recent efforts to unravel the microscopic mechanisms for various types of MITs in correlated materials is provided. Research has focused on transition metal oxides (TMOs), but transition metal chalcogenides have also been studied. Along the way, a new class of MIT materials is discovered, the so-called relativistic Mott insulators in 5d TMOs. Distortions in the $MO_6$ (M = transition metal) octahedron are found to have a large and peculiar effect on the band structure in an orbital dependent way, possibly paving a way to the orbital selective Mott transition. In the final section, the character of the materials suitable for applications is summarized, followed by a brief discussion of some of the efforts to control MITs in correlated materials, including a dynamical approach using light.

## 1. Introduction

The interplay between charge, spin, orbital, and lattice degrees of freedom in correlated materials often leads to various novel phases such as high-temperature superconductivity,[1–3] colossal magnetoresistance,[4,5] and multiferroicity.[6–8] Among those phases and transitions between them, the metal–insulator transition (MIT) is a well-known phenomenon that can exhibit many orders of magnitude change in the resistivity.[9,10] The transition occurs over small variation in external parameters such as temperature, magnetic field, and pressure. The MIT has been one of the most attractive subjects in correlated materials research, with its rich research history dating back to 1930s.[9,11,12] While it is a novel phenomenon and is important in its own right, the large change in the resistivity is also a desirable trait needed for device applications. For example, the MIT in vanadium oxides is now being used as a temperature sensitive switch in fire detectors.[13–15] In addition, a new form of transistor, i.e., the Mott transistor,[16] is being discussed.

What causes such a drastic change in resistivity is an intellectually interesting question and various mechanisms have been proposed for different systems, e.g., the Mott transition[17] and the Slater mechanism.[18] Moreover, MIT systems with yet different mechanism are still being discovered. Therefore, a comprehensive understanding of MIT phenomena in correlated materials is a challenging task and would have significant impact on correlated materials research. On the application side, comprehensive understanding of the MIT properties could be useful in finding materials with appropriate parameters. That is, one hopes to adjust the material parameters so that one can use the critical region in the vicinity of the (multi) critical points along the phase boundaries and that the phase boundaries are located within the accessible (operating) range of external parameters. However, a general understanding of MITs in correlated materials remains one of the major unsolved problems in condensed matter physics.[19,20]

At the core of the investigation of the MIT mechanism lie electronic structure studies by spectroscopic techniques. While theoretical methods such as density functional theory in general could be used to understand electronic transport properties of materials, accurate calculation of electronic structures of correlated materials is difficult because the "bare" electronic band structure is deformed by the electron–electron (el–el) correlation. Spectroscopic techniques can provide vital information on the electronic structure and help us to understand the MIT

S. Y. Kim, M.-C. Lee, Dr. G. Han, Dr. M. Kratochvilova, S. Yun,
Prof. J.-G. Park, Prof. C. Kim, Prof. T. W. Noh
Center for Correlated Electron Systems
Institute for Basic Science
Seoul 08826, Republic of Korea
E-mail: changyoung@snu.ac.kr
S. Y. Kim, M.-C. Lee, Dr. G. Han, Dr. M. Kratochvilova,
S. Yun, Prof. J.-G. Park, Prof. C. Kim, Prof. T. W. Noh
Department of Physics and Astronomy
Seoul National University
Seoul 08826, Republic of Korea
Prof. S. J. Moon
Department of Physics
Hanyang University
Seoul, Republic of Korea
Dr. C. H. Sohn
Materials Science and Technology Division
Oak Ridge National Laboratory
TN 37831, USA

mechanisms. We have made continued efforts to understand MIT phenomena in correlated materials through studies based on various spectroscopic methods. In this report, we overview the progress in our research on the MIT. We start with introducing various material groups that are categorized by the origin of the MIT along with the description of how the two major spectroscopic techniques, i.e., angle-resolved photoemission spectroscopy (ARPES)[2] and optical spectroscopy,[21] are used in the studies. Among many materials we have studied, we choose material groups that are recently found or have experienced renewed interest: 3d-, 4d-, and 5d-transition metal oxides (TMOs) Mott insulators, 5d-transition metal (TM) pyrochlores, and MIT materials with emerging new structure patterns. We will discuss the issues in each group and try to address them in relation to the MIT mechanism. In the final section of this article, we provide a summary on the properties of the materials we have studied suitable for applications[161,164–168,190–193,196] and brief discussion on possible ways to obtain desirable parameters. We hope that the information we gathered through our studies will be important in synthesizing MIT materials for future device applications.

## 2. A Survey on Different Types of Metal–Insulator Transitions

There can be various causes for the MIT and, as a result, materials can go through the MIT in different ways. Therefore, it is useful to have a survey on the material groups categorized by the driving forces of the MIT and the resulting emergent phenomena as shown in **Table 1**. The classical formula for electrical conductivity given by Drude is expressed as

$$\sigma = ne^2\tau/m* \tag{1}$$

where $n$, $m*$, and $\tau$ are the carrier number, carrier effective mass, and scattering time, respectively.[22] The simple equation shows that the conductivity will vanish when $n$ or $\tau$ goes to zero, or when $m*$ becomes infinite. We discuss the driving force within each group and the way a material becomes an insulator in terms of the parameters in Equation (1).

**Table 1.** Various types of MIT with the origin of the transition as well as resulting emergent phenomena.

| Driving force | MIT mechanism(s) | Emergent phenomena |
|---|---|---|
| Structure change | $n \rightarrow 0$ | Band insulator |
| AFM magnetic ordering | $n \rightarrow 0$ | Slater insulator |
| Disorder (impurity) | $\tau \rightarrow 0$ | Anderson insulator |
| el–phonon interaction (polaron) | $\tau \rightarrow 0$ | Colossal magnetoresistance |
| el–el correlation | $m* \rightarrow \infty$ ($n \rightarrow 0$) | Mott insulation |
| +Orbital degeneracy | Band dependent $m* \rightarrow \infty$ | Orbital-selective Mott transition |
| +Spin–orbit coupling | $m* \rightarrow \infty$ | $J_{eff} = 1/2$ relativistic Mott insulator |
| All-in-all-out AFM ordering | $n \rightarrow 0$ | AIAO AFM semimetal |

**Je-Geun Park** obtained his B.Sc. (1988) and M.Sc. (1990) degrees in physics from Seoul National University and the Ph.D. (1993) in physics from Imperial College, London. He is currently professor of the Department of Physics and Astronomy at Seoul National University and associate director at the Center for Correlated Electron Systems, Institute for Basic Science. Prior to taking his current posts, he was founding director of the Center for Korean J-PARC Users at Seoul National University, and professor and SKKU Fellow of Department of Physics at Sungkyunkwan University. His research is focused on the physical properties of strongly correlated electron systems, in particular the magnetic properties using neutron and X-ray irradiation.

**Changyoung Kim** received his Ph.D. degree from the Department of Applied Physics at Stanford University in 1994. From then, he worked at the Stanford Synchrotron Laboratory (until 2001) and at Yonsei University (until 2015). He joined the Department of Physics and Astronomy at Seoul National University in 2015. He is also an associate director of the IBS Center for Correlated Electron Systems. His research interests include orbital angular momentum effects under inversion symmetry breaking, the metal–insulator transition, transition metal oxides and unconventional superconductivity. In general, he is interested in electronic structure studies of correlated materials.

**Tae Won Noh** received his Ph.D. degree from the Department of Physics at Ohio State University in 1986. From then, he worked at Cornell University. In 1989 he joined the Department of Physics and Astronomy at Seoul National University. He is currently director of the IBS Center for Correlated Electron Systems (CCES). His research interests include metal–insulator transitions, electron correlation effects, spin–orbit coupling effects, transition metal oxides, and ferroelectricity. His group grows oxide thin films and performs optical spectroscopy measurements. He is also interested in physics and applications of nonvolatile memories, such as FeRAM and RRAM.

**ADVANCED
SCIENCE NEWS**

www.advancedsciencenews.com

**ADVANCED
MATERIALS**

www.advmat.de

The first one is the simple band insulator in which case bands below a gap are completely filled while bands above the gap are empty. Whether the bands below the gap are filled or not critically depends on the overlap between bands. In that sense the MIT can be driven by the crystal structure with $n \rightarrow 0$. The role of the crystal lattice can be played by a magnetic order, usually an antiferromagnetic (AFM) one. The extra order causes band folding with a smaller Brillouin zone (BZ), resulting in gap opening at the BZ boundary. The insulating state caused by an AFM order is called a Slater insulator.[18] As AFM is usually accompanied by strong el–el correlation, it is rather difficult to attribute the insulating state solely to an AFM order. Active search for a true Slater insulator is still continuing.

Disorder and impurity can also cause transition to insulating states, especially at a low temperature, through the mechanism known as Anderson localization.[23,24] Disorders and impurities can generate localized impurity potentials and these local potentials can trap carriers at a low temperature. The trapped carriers are immobile and the system becomes an insulator effectively by the vanishing scattering time ($\tau \rightarrow 0$). The well-known characteristics of the Anderson localization is logarithmic behavior of the temperature-dependent resistivity in the low-temperature region.[25] Vanishing scattering time can also be caused by strong electron–phonon (el–ph) coupling. When el–ph coupling is strong, electrons can severely deform the lattice, resulting in the formation of polarons.[26] Well-known examples of polaronic insulators are maganites with colossal magnetoresistance.[27,28]

Mott transition is an MIT phenomenon caused by strong el–el correlation.[10] When the correlation increases, it becomes energetically favorable for the electrons to reside in localized wave functions, eventually driving the system to an insulating state when the correlation becomes strong enough. This Mott MIT has been one of the most important topics in solid-state physics and is found in a variety of materials with strong correlations, especially in 3d TMOs.[19,29] Theoretical studies based on dynamical mean field[30,31] show that the Mott transition occurs when the effective mass becomes infinite ($m^* \rightarrow \infty$). However, verification of such mechanism by direct experimental methods has not been properly done.

It was theoretically suggested that the Mott transition can occur in an orbital-dependent way when a material has an orbital degree of freedom (multiband systems) in addition to the strong el–el correlation. That is, while a band from an orbital goes through the Mott transition, other bands may remain in metallic states. Such phenomenon is referred to as orbital selective Mott transition (OSMT).[32] OSMT was originally proposed for the MIT in $Ca_{2-x}Sr_xRuO_4$[33] and experimental observation of OSMT in the same system has been claimed later.[34,35] In spite of the claims, indisputable experimental observation as well as clear theoretical understanding appears to be still a distance away.

Meanwhile, it was found that combination of strong spin–orbit coupling (SOC) and el–el correlation can lead to a new type of Mott insulator known as relativistic Mott insulator, first discovered in an iridium compound $Sr_2IrO_4$.[36] As discussed in the main text, relativistic Mott insulators require strong SOC as well as the usual electron correlation, and are in a $J_{eff} = 1/2$ state, instead of the usual $S = 1/2$, due to the strong SOC. Relativistic Mott insulators are expected to become insulating via diverging

effective mass ($m^* \rightarrow \infty$) as they are a type of Mott insulator. While the $J_{eff} = 1/2$ AFM state is interesting in its own, its similarity to the $S = 1/2$ AFM state in parent compounds of curate superconductors made it even more interesting due to the possibility of the $J_{eff} = 1/2$ unconventional superconductivity.[37,38]

Finally, there are cases where the MIT is coupled to a magnetic order. In recent years, particular attention has been paid to $A_2B_2O_7$ (A = rare earth ion, B = Ir, Os) type 5d pyrochlore compounds that exhibit a novel magnetic order, known as all-in-all-out (AIAO) order.[39,40] In the AIAO configuration, all the spins of a 5d TM tetrahedron point inward while spins of neighbor tetrahedra point outward. The MIT in these materials occurs with the AIAO magnetic order, suggesting that the magnetic order could be the cause of the MIT. These materials have drawn much attention lately due to the possibility of novel states such as Weyl semimetal and quantum criticality.[39,41,42] However, how the AIAO magnetic order is related to the MIT was not clearly addressed.

We have surveyed different types of MITs. Even though the list in Table 1 does not cover all MIT types, it should include most of the major material groups. An important message is that, as mentioned at the beginning of this section, there are diverse material groups with different origins for the MIT, giving us a variety of possibilities for controlling the MIT.

## 3. Experimental Techniques

Various experimental techniques are involved in our studies on MIT materials, including spectroscopic methods, scattering, thin film, and single crystal growth. Among these techniques, spectroscopic methods played a major role in our studies. Before we discuss the progress in our research, we provide descriptions of the two major spectroscopic techniques, i.e., ARPES and optical spectroscopy. Only brief descriptions that are needed for the discussion in the report are given. For detailed and thorough descriptions of the two techniques, readers may refer to review articles.[2,43]

In addition to ARPES and optical spectroscopy, other techniques were used. Neutron scattering, muon spin rotation ($\mu$SR), and X-ray diffraction were used to investigate the exotic patterns in MIT materials (Section 4.3). Ultrafast spectroscopy is a technique for the study of photoinduced MIT (Section 5.2). These techniques are briefly introduced in the following sections.

### 3.1. Angle-Resolved Photoemission Spectroscopy

What determines a system to be a metal or insulator is whether it has mobile electrons or not. In view of the electronic structure, electrons are mobile if there is a finite density of states at the Fermi energy ($E_F$), that is, if a band (or bands) crosses $E_F$. Therefore, the band structure bares critical information on the MIT. For example, in regard to Equation (1), one can obtain the effective mass $m^*$ from the band dispersion near $E_F$ as well as the carrier density $n$ from the Fermi surface (FS) volume. Therefore, the question is how one can measure the band structure near $E_F$.

**ADVANCED
SCIENCE NEWS**
www.advancedsciencenews.com

**ADVANCED
MATERIALS**
www.advmat.de

The most direct way to measure the electronic structure is through ARPES. The principle behind ARPES is the famous Einstein's photoelectric effect.[44] When monochromatic light (photons) impinges on a material, it can emit photoelectrons containing the information on both energy and crystal momentum in the material. According to the energy conservation law, the kinetic energy $E_{kin}$ of the photoelectron is written as

$$E_{kin} = h\nu - \Phi - |E_B| \tag{2}$$

where $h\nu$ is the photon energy, $\Phi$ is the work function, and $E_B$ is the binding energy of the initial state. As for the momentum, the case is more complicated but it can be simplified with the condition that the photon momentum is negligible, which is the case for the usual low photon energy ARPES ($h\nu < 1000$ eV). With the momentum conservation law, the parallel component (to the crystal surface) of the crystal momentum $\vec{k}_\parallel$ in the initial state can be obtained by

$$\vec{k}_\parallel = \frac{1}{\hbar}\sqrt{2mE_{kin}}\sin\theta \tag{3}$$

where $\theta$ is the polar angle of the photoelectron (**Figure 1**a). The perpendicular component of the crystal momentum is not conserved due to the transitional symmetry breaking across the crystal surface[45] but can be obtained by considering the inner potential of the system which requires a photon energy scan. However, in the cases of low dimensional systems, only $\vec{k}_\parallel$ information is needed. Therefore, by analyzing the energy and emission angle of photoelectrons, one can obtain the electronic band structure of the occupied states as schematically shown in Figure 1a. Figure 1b shows typical ARPES data along a certain momentum direction in the Brillouin zone. Data can be

obtained over the full BZ, and the spectral weight at $E_F$ gives us an FS map such as the one shown in Figure 1c.

ARPES is a powerful technique for electronic structure studies of correlated materials, especially for multiband systems.[2,35,46,47] While el–el correlation may not affect the carrier density $n$, it can change the effective mass $m^*$ of the band. In the case of the usual parabolic dispersion, $m^*$ can be obtained from the Fermi velocity $v_F$ by

$$m^* = \hbar k_F / v_F \tag{4}$$

where $k_F$ is the Fermi wave vector and $v_F = (dE(k)/dk)|_{k=k_F}$ as shown in Figure 1b.[48] The mass enhancement of each band can be determined by comparing the measured effective mass with the bare band mass $m_b$ obtained by the density functional theory[49]

$$m^*/m_b = v_{F,cal}/v_{F,ARPES} \tag{5}$$

We note that this method is only for the bands crossing the Fermi level and thus cannot be applied to the bandgap renormalization in semiconductors. It is the most direct way to obtain the mass enhancement in multiband systems in a band-dependent way. Other quantities such as the heat capacity coefficient $\gamma$,[50] magnetic susceptibility $\chi$,[51] and resistivity $T^2$-coefficient $A$[52] provide only the average mass enhancement. Therefore, ARPES should be a suitable tool to investigate not only the usual Mott MITs in 3d TMOs (Section 4.1) but also OSMTs in 4d- and 5d-TMOs (Section 4.2).

### 3.2. Optical Spectroscopy

Optical spectroscopy is a powerful probe to investigate carrier dynamics and electronic structure of solids. Typically, a white light from terahertz (THz) to ultraviolet (UV) frequency is shone on the sample and the response is measured. Through a proper treatment (e.g., Fresnel's equation and/or Kramers–Kronig relations) of the reflected/transmitted light from the sample, various optical constants of materials can be obtained.[53,54] While they can provide information averaged over the whole $k$-space, their bulk sensitivity (the typical probing length is on the order of micrometers) is a clear advantage over surface-sensitive low-energy probes such as ARPES and scanning tunneling spectroscopy in investigating the bulk properties of materials.

The electronic response probed by optical spectroscopy is usually represented by the optical conductivity $\tilde{\sigma}(\omega)[= \sigma_1(\omega) + i\sigma_2(\omega)]$. $\tilde{\sigma}(\omega)$ is a measure of the rate at which particle–hole pairs are created by photon with an energy $\hbar\omega$ and it reflects absorptive ($\sigma_1$) and inertial responses ($\sigma_2$). The optical conductivity contains instrumental information on the charge dynamics and electronic structure, and therefore can provide valuable information on the MIT phenomena in strongly correlated electron systems. As a prototypical example of the MIT, we display $\sigma_1(\omega)$ of $VO_2$ in **Figure 2**a,b.[187] At $T < T_c$, the optical conductivity is zero below the optical gap of about 0.6 eV, indicating there is no free carrier (insulating phase) (Figure 2a). Upon increasing the $T$, however, $VO_2$ undergoes an MIT and the spectrum changes drastically; $\sigma_1(\omega)$ at $T > T_c$ clearly shows a metallic signal with a Drude peak, i.e., light
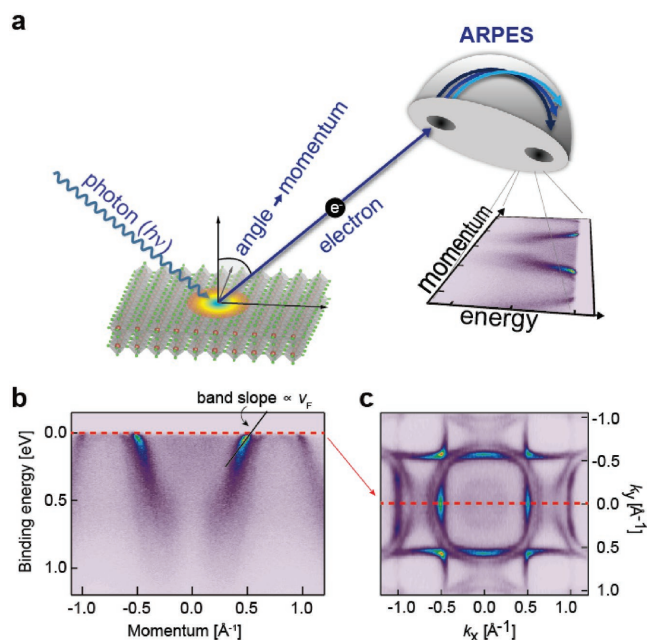


**Figure 1.** Introduction to ARPES. a) Schematic illustration of ARPES. b) $Sr_2RuO_4$ Fermi surface. c) ARPES data of $Sr_2RuO_4$.
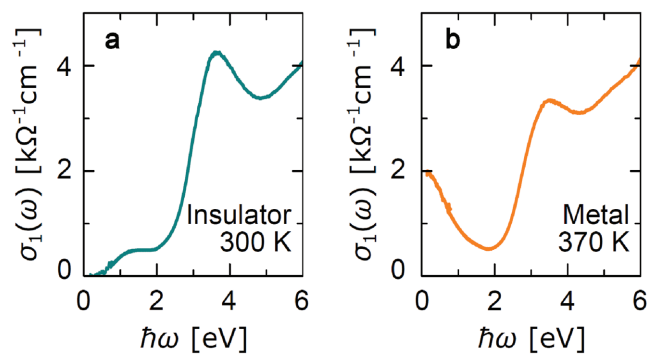
**Figure 2.** Real part of the optical conductivity $\sigma_1(\omega)$ of the $VO_2$ thin film[187] from: a) insulating and b) metallic states.



**Figure 3.** a–c) Simplified schematic diagrams of the Mott transition for various $U$ sizes. a) When U is small, since usually screened by itinerant electrons in a normal metal, a "bare" bandwidth is only determined by atomic periodic (that is, Bloch) potential. b) When $U$ is as large as $t$, an electron has either itinerant or localized properties. The itinerant part forms the QP band (a sharp peak at the center) while the localized part forms the incoherent bands (two broad humps). c) When $U$ is larger than the critical value, $U_c$, the spectral weight of QP band is entirely transferred to the incoherent bands, thus the system becomes an insulator (for more details, see the main article). d) Appearance/disappearance of the QP in the metallic/insulating states near the Mott transition in $NiS_{2-x}Se_x$. e) Appearance/disappearance of the QP across the temperature-dependent Mott transition in $Ni_{1.5}Se_{0.5}$.[78]

absorption spectrum described with a Lorentzian oscillator centered at zero frequency (Figure 2b).[53] Both cases show optical transitions above 1.5 eV, which provides information on the underlying electronic structure of $VO_2$.[55]

When dealing with a system having strong el–el interactions, the extended Drude model (EDM) is frequently used. It is based on treating the damping term frequency-dependent.[56] By applying the EDM model, the frequency-dependent scattering rate $1/\tau(\omega)[= Re\{\omega_p^2/4\pi\tilde{\sigma}(\omega)\}]$ and mass enhancement $m*(\omega)/m_b[= Im\{\omega_p^2/4\pi\tilde{\sigma}(\omega)\}$ of electronic excitations can be obtained.[43,56] Here, $m_b$ is the band mass and $\omega_p$ is the plasma frequency.[53,54,57] The EDM has been used in the studies of numerous correlated materials including high transition temperature (high-$T_c$) superconductors,[58,59] heavy fermion systems,[60] and aforementioned vanadate system ($VO_2$, $V_2O_3$).[55]

More advanced methods with very high spatial/time resolution have been developed recently. For instance, the near-field infrared imaging method allows a nanometer-scale spatial resolution,[43] which provided a new insight on the percolation process in $VO_2$[61] as well as decoupling of structure and electronic transitions in $V_2O_3$.[55,62,63] On the other hand, pump–probe spectroscopy can give optical perturbation on the system and measure the optical constant change with a femtosecond time resolution. The optical perturbation can induce novel transient state, and additional information in time dimension allows decoupling of various effects coexisting in correlated materials.[64–67]

# 4. Experimental Studies of Metal–Insulator Transitions in Correlated Materials

## 4.1. Mott Transitions in 3d Transition Metal Compounds

### 4.1.1. Theory of the Mott Transition

Within the conventional single-electron picture, metals and insulators are classified by the valence band filling.[22] In the case of an insulator, the valence band is completely filled while a metal has partially filled bands. The theory has successfully predicted many properties of materials. However, as early as in 1937, de Boer and Verwey reported that some TMOs are insulators even though they were predicted to have partially filled d-bands.[11] In an attempt to explain the experimental results, Mott and Peierls proposed that el–el correlation can turn the
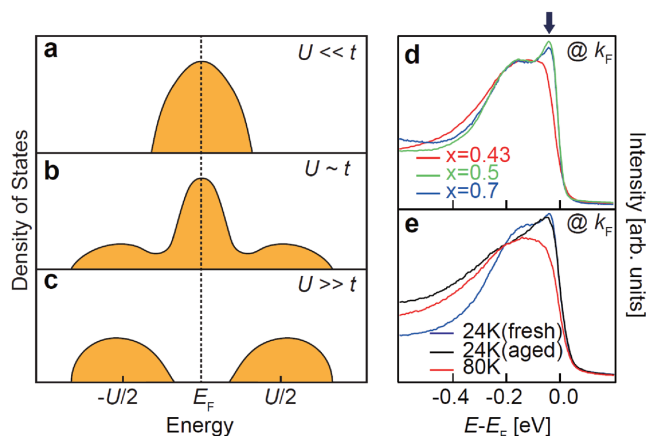
material into an insulator.[68] Although the proposal can explain general aspects of the insulating state, how a metal actually becomes a Mott insulator has not been clearly understood.

Recently developed dynamical mean field theory (DMFT)[30,31] has succeeded in describing this situation (**Figure 3**a–c). When the el–el Coulomb repulsion energy $U$ is much smaller than the hopping energy $t$ ($U << t$), the freely propagating electrons form a bare band with its bandwidth $W$ solely determined by the periodic potential and proportional to $t$ ($W = 2zt$, where $z$ is the number of nearest neighbors) (Figure 3a). As $U$ increases, the electron motion slows down by the el–el interaction. The slowly moving electron is equivalent to a particle with a larger effective mass without interaction and is called a quasiparticle (QP). When $U$ becomes as large as $t$ ($U \sim t$), electrons have both itinerant and localized properties. The itinerant part forms the QP band (the sharp peak at the center in Figure 3b) while the localized part forms the incoherent bands (two broad humps), that is, some of the spectral weight is transferred from the QP band to the localized incoherent bands. When $U$ becomes significantly larger than $t$ ($U >> t$), the effective mass of the QP diverges and the QP spectral weight is entirely transferred to incoherent bands (lower and upper Hubbard bands) (Figure 3c). This type of MIT is referred to as the bandwidth-controlled MIT because its control parameter can be written as $U/W$.

### 4.1.2. Experimental Confirmation of the Theory

The key predictions of DMFT for the Mott transition are the existence of the QP band between the Hubbard bands (as illustrated in Figure 3b) and renormalization of the QP band. Even though the behavior of the predicted QP band is an important signature

**ADVANCED
SCIENCE NEWS**

www.advancedsciencenews.com

**ADVANCED
MATERIALS**

www.advmat.de

of the Mott transition, it has been a challenge to observe the QP peak directly. For instance, there have been great efforts to observe the QP in $V_2O_3$, a well-known Mott transition material.[9,10] However, the observed intensity of the band at $E_F$ was not as high as the estimated one from the theory, probably due to extrinsic reasons.[69–72] The predicted QP was observed by using high-energy photoemission spectroscopy but only momentum integrated results have been obtained.[73] Momentum-resolved data was obtained for $NiS_{2-x}Se_x$,[74,75] and the peak near $E_F$ was assigned to the QP[76] (the peak in momentum-integrated spectrum has also been called the QP peak in many cases[9,10] but here we use the definition that momentum-resolved peak is the QP peak[45] while the momentum-integrated peak is the QP band). However, this peak remained even in the insulating regime, casting some doubt on the validity of such assignment. Recently, a possibility for surface origin of the peak was raised.[77] To avoid such issues, soft X-ray ARPES has been used to obtain bulk sensitive data.[77] However, the QP was buried in the incoherent band and could not be clearly resolved.

Recent ARPES experiment by Han et al. utilizing low photon energy and high resolution has revealed a clear QP peak in $NiS_{2-x}Se_x$.[78] Figure 3d shows energy distribution curves at the $k_F$ for various dopings. A sharp and narrow QP peak near $E_F$ is observed for the metallic phases ($x = 0.5$ and $0.7$) while the peak loses its intensity for an insulating system ($x = 0.3$). We may also study the behavior of the QP peak across the MIT by exploiting the MIT temperature $T_c = 50$ K for $NiS_{1.5}Se_{0.5}$. As shown in Figure 3e, we observe complete disappearance of the QP peak when the temperature increases to 80 K, well above $T_c$. Upon cooling down the system from 80 to 24 K, the QP peak reappears even though somewhat weaker due to the aging effect. The reappearance of the QP peak assures that the peak is the key feature of the MIT and thus QP predicted by the theory.

Despite the successful observation of a clear QP peak, divergence of the QP mass has not been observed in real MIT materials. In the high-pressure experiment on $V_{2-x}O_3$, the specific heat coefficient, proportional to the effective mass according to the Fermi liquid theory,[22] was found to be greatly enhanced near the MIT.[79] The maximum value, however, was much smaller than that of heavy fermion materials despite the fact that the coefficient is additionally enhanced by the AFM order fluctuation. On the other hand, $NiS_{2-x}Se_x$ provides a better platform to investigate the divergent effective mass issue. Since the AFM transition is far from the MIT,[80,81] the fluctuation effect should be already suppressed near the MIT. Moreover, the crystalline and magnetic structures are retained across the MIT, and thus one only has to consider the electronic effect.[82,83] Although it has been claimed that the effective mass of $NiS_{2-x}Se_x$ diverges near the MIT in the study using Soft X-ray ARPES,[77] the result is not consistent with the specific heat result.[84] Therefore, controversy still remains over whether the mass diverges or not. In the work of Han et al., it was clearly shown that the effective mass does not diverge.[78]

### 4.1.3. Structure-Assisted Mott Transition and its Control

The reason why the mass divergence is not observed in real systems is that there are interactions between electrons and other

degrees of freedom[10]; only pure electronic effect is considered in the theoretical prediction for the Mott transition. With the additional interactions, the metallic state may turn into an insulating state before the effective mass hits the divergence, in which case a symmetry breaking is usually involved. In particular, a structural transition accompanies the MIT in many cases to reduce the lattice instability. Coupling with other degrees of freedom works as an obstacle in studying the electronic effects. However, we note that it can also be used as a parameter to control the MIT, a beneficial aspect for applications.

How to control the MIT is also an important question. One of the easiest ways is to apply pressure.[85–88,189,194,195,199] The atomic distance reduced by pressure increases an overlap between wave functions and thus the bandwidth. In a similar manner, we can apply chemical pressure, namely, we replace an ion in the material with a larger or smaller ion of the same group as is the case for $NiS_{2-x}Se_x$.[76,89] Another way is to change the bandwidth through modification of the crystal structure. $VO_2$ undergoes the MIT with V–V dimerization which lifts a band at the Fermi level.[90] In many TMOs, the bandwidth is reduced with distortion of $MO_6$ (M = TM) octahedron. In the $MO_6$ octahedron structure, five degenerate d orbitals are split into doubly degenerate $e_g$ orbitals and triply degenerate $t_{2g}$ orbitals. Jahn–Teller distortion, for example, reduces the bandwidth by breaking the degeneracy of $e_g$ and $t_{2g}$ orbitals.[91] Octahedral rotation is also one of the ways to control bandwidth. In a traditional sense, octahedral rotation reduces bandwidth by reducing the overlap between M–O–M orbitals. However, controversy remains as to whether this effect is large enough to ignite the MIT. Representative examples of the MIT that involve octahedral rotation are in $Sr_{1-x}Ca_xVO_3$[48,92,93] and $Ca_{2-x}Sr_xRuO_4$.[34,94–96]

Although extensive studies have been made to understand the Mott transition, there still remain many unresolved issues. In particular, it is important to find a system where MIT occurs only with el–el correlation, without coupling to other degrees of freedom. This is to discover a yet elusive system that shows the mass divergence. Studies on materials with a single-band could be the answer as the divergence was predicted in the single band Hubbard model. In an application point of view, how to control the Mott transition is an important issue. As an example, research is underway to control MIT through the Joule heating since the Mott transition shows a large resistance difference even with a small temperature change.[16]

### 4.2. Orbital Selective Mott Transitions in 4d Transition Metal Oxides

In the 4d electron systems, the octahedral rotation changes the band structure more dramatically than in a 3d electron system. $Ca_{2-x}Sr_xRuO_4$, another example of octahedron rotation and tilt-induced MIT, has dawn much attention due to the possibility for an OSMT.[33,34] In $Sr_2RuO_4$ (**Figure 4**a), the Ru ion has four electrons in the $t_{2g}$-subshell, and the upper $e_g$-subshell is completely empty. The partially filled $t_{2g}$-subshell makes the $Sr_2RuO_4$ a covalent metal. Since the $RuO_6$ octahedron is slightly elongated in the $c$-axis direction, in-plane $d_{xy}$ and out-of-plane $d_{xz}$ and $d_{yz}$ orbitals produce small energy splitting. The $d_{xy}$ orbital, however, has twice the bandwidth of the $d_{xz}$
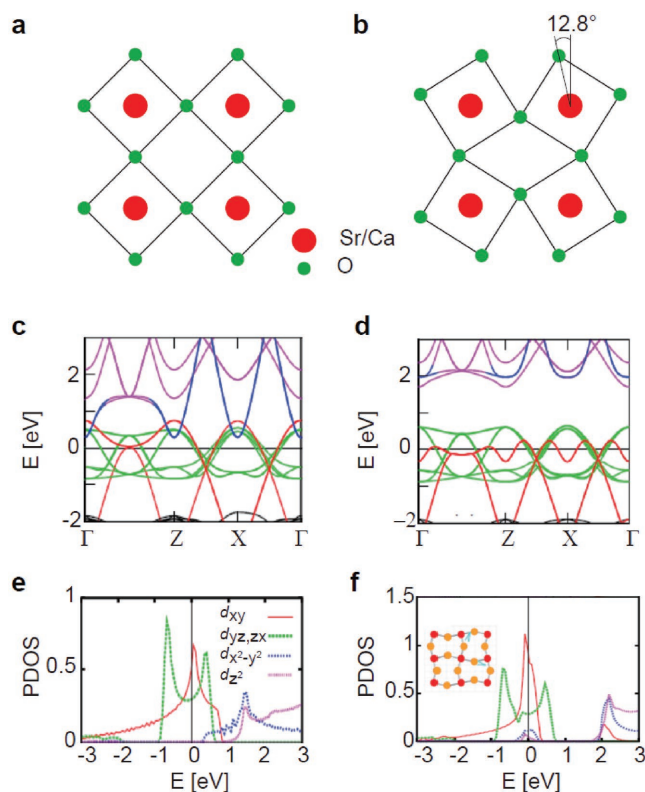
**Figure 4.** a,b) Schematic atomic structure of the Sr–O plane in $Sr_2RuO_4$ with 0° and 12.8° octahedral rotation, respectively. c,d) Calculated band structures and e,f) projected density of states near $E_F$ for $Sr_2RuO_4$ using the $\sqrt{2} \times \sqrt{2} \times 2$ supercell for the 0° and 12.8° octahedron rotation. Adapted with permission.[96] Copyright 2007, American Physical Society.

or $d_{yz}$ orbital. When Sr in $Sr_2RuO_4$ is replaced by an isovalent Ca ion, it evolves to a correlated metal ($0.2 < x < 0.5$) and is eventually transformed into a Mott insulator ($x < 0.2$).[96] In the $0.5 < x < 2$ range, $RuO_6$ octahedra undergo an in-plane rotation (Figure 4b), resulting in a significant increase in magnetic susceptibility and heat capacity at low temperatures.[97] In the conventional scheme, the bandwidths of $d_{xz}$ and $d_{yz}$ bands decrease due to the in-plane rotation while $d_{xy}$ retains a broad bandwidth. Based on such argument, a possibility for band dependent transition or OSMT was proposed theoretically.[33]

Lee et al. showed the orbital-selective mass enhancement by analyzing the optical conductivity from $Ca_{2-x}Sr_xRuO_4$ within the EDM model.[34] Contrary to the case of the specific heat coefficient $\gamma$ which shows a large enhancement with increasing Ca concentration, the $m^*/m_b$ obtained from the EDM analysis did not show a significant change. The difference in the responses of $\gamma$ and $m^*/m_b$ implies that the three $t_{2g}$ bands have distinct spectral weights and effective masses. To explain the experimental observation, a large mass enhancement in the $d_{xz}/d_{yz}$ bands was proposed.[33] However, it could not accurately account for the optical spectra. On the other hand, Lee et al. suggested that the $d_{xy}$ band is largely renormalized, which explains both optical spectroscopy and the specific heat coefficient results. These results therefore call for a new OSMT model for the $Ca_{2-x}Sr_xRuO_4$ system.

The possibility for OSMT in $Ca_{2-x}Sr_xRuO_4$ has inevitably led to ARPES studies.[98] However, it turned out to be difficult to obtain a clear band structure due to the disorder effect from Ca substitution. On the other hand, $Sr_2RhO_4$ provides an opportunity to reveal the effect of octahedral rotation without disorder[99] since it already has an in-plane octahedron rotation as in $Ca_{2-x}Sr_xRuO_4$. Although $Sr_2RhO_4$ has more electrons than $Sr_2RuO_4$, it is still suitable for a comparative study because $Sr_2RhO_4$ shares many similarities with $Sr_2RuO_4$. Structurally, $Sr_2RhO_4$ has a layered perovskite $K_2NiF_4$ structure with octahedra elongated in the same way as $Sr_2RuO_4$. $Sr_2RhO_4$ has one more electron than $Sr_2RuO_4$, filling the $t_{2g}$ manifold with five electrons. Therefore, the electronic structure of $Sr_2RhO_4$ is expected to be similar to that of $Sr_2RuO_4$ with a rigid shift. However, Kim et al. discovered that measured $Sr_2RhO_4$ FS is drastically different from that of $Sr_2RuO_4$.[99] The biggest difference is that the $d_{xy}$ band is missing in the $Sr_2RhO_4$ FS map. The result has led to the understanding that $d_{xy}$ and $d_{x^2-y^2}$ bands hybridize and open a large gap, pushing the $d_{xy}$ band below $E_F$.

Applying the mechanism to the $Ca_{2-x}Sr_xRuO_4$ case, octahedral rotation is expect to affect $d_{xy}$ orbital rather than $d_{yz}/d_{xz}$ orbitals. Ko et al.[96] showed that the strong mass enhancement in $Ca_{2-x}Sr_xRuO_4$ is not due to localized $d_{yz}/d_{xz}$ but due to the change in the $d_{xy}$ band from hybridization between $t_{2g}$ and $e_g$ bands. Figure 4 shows a calculated band structure and projected density of states (PDOS) of $Sr_2RuO_4$ with a rotation angle of 12.8° (same rotation angle as in $Ca_{1.5}Sr_{0.5}RuO_4$). In spite of the energy difference of about 3 eV between $t_{2g}$ and $e_g$ bands from crystal field splitting, the bottom of the $d_{x^2-y^2}$ band is located at only 0.3 eV above $E_F$ due to the large bandwidth. When octahedral rotation occurs, the original 2D BZ of $1 \times 1$ square lattice turns into $\sqrt{2} \times \sqrt{2}$ lattice with a 45° rotation. The $\sqrt{2} \times \sqrt{2} \times 2$ supercell leads to an overlap between the $d_{x^2-y^2}$ and $d_{xy}$ bands (Figure 4c). As in $Sr_2RhO_4$, hybridization of $t_{2g}$ and $e_g$ bands in $Ca_{2-x}Sr_xRuO_4$ pushes the $d_{xy}$ band to higher binding energy side (Figure 4d) and reduces the bandwidth by 40%. The bandwidth reduction in $d_{xy}$ from the hybridization effect is much larger than the 10% reduction in $d_{yz}/d_{xz}$ bandwidth expected from the rescaled hopping energy. These are clearly demonstrated in Figure 4e,f where the calculated PDOS for 0° and 12.8° rotations is shown. For the 12.8° case, the $d_{xy}$ band is affected by the rotation, resulting in a reduction in the $d_{xy}$ bandwidth. On the other hand, the bandwidth of $d_{yz}/d_{xz}$ is not much affected. Even though the actual situation is more complicated due to the tilt motion in the OSMT range ($0.2 < x < 0.5$), the above picture catches the key feature, that is, why the $d_{xy}$ band is more renormalized than the $d_{yz}/d_{xz}$ bands. In a recent report on ARPES investigation of $Ca_{1.8}Sr_{0.2}RuO_4$, it was seen that $d_{xy}$ band was missing.[35] The observation clearly suggests that OSMT indeed occurs in the $d_{xy}$ band, which is consistent with our picture. Based on these observations, one can deduce that the large effective mass is due to hybridization between $t_{2g}$ and $e_g$.

### 4.3. Relativistic Mott Insulating States in 5d Transition Metal Oxides

#### 4.3.1. 5d Transition Metal Oxides

Until a decade ago, the electronic correlations via the Coulomb repulsion $U$ was often neglected in 5d TM-based compounds.

ADVANCED
SCIENCE NEWS
www.advancedsciencenews.com

ADVANCED
MATERIALS
www.advmat.de

In 3d TM-based compounds where electrons are well localized in 3d orbitals, it is natural to consider the strong Coulomb interaction of electrons. Indeed, the typical energy scale of $U$ in 3d TM compounds is large, ranging from 4 to 7 eV. On the other hand, the bandwidth of d-orbital states ($W$) or hopping integral $t$, is around 1–2 eV in 3d TM.[10,17,100] The large $U$ ($U/W > 1$) can drive the system into Mott insulating states as discussed previously. On the other hand, the electrons tend to be delocalized in TM with a large atomic number. The extended nature of 5d TMs reduces $U$ and increases $W$. The typical $U$ values of 5d TM are in the range of 0.5–2 eV while $W$ in 3–4 eV range.[36,101,102] Because the Coulomb repulsion is not strong enough to open a Mott gap ($U/W < 1$), most 5d TM compounds should be metallic within the classical band picture or in the simple Mott picture.

However, the insulating behaviors have been found in some of 5d TM compounds with partially filled valence state. To understand the nature of the insulating state of 5d TM compounds, a new insight was required. A recent study of $Sr_2IrO_4$, a relativistic Mott insulator, provided such insight and opened the fast-growing field of 5d TM compounds.[36,103] Since then, 5d TM (e.g., Re, Os, Ir) compounds have attracted much attention,[36,102,104–106] as in the case of the well-studied 3d TM systems (e.g., V, Mn, Ni, and Cu).[10,17,55,107]

### 4.3.2. The Insulating Mechanism of $Sr_2IrO_4$

$Sr_2IrO_4$ is an adequate system to investigate the insulating mechanism of 5d TM compounds. $Sr_2IrO_4$ has the $K_2NiF_4$ structure, and is the $n = 1$ member of the Ruddlesden–Popper series iridate ($Sr_{n+1}Ir_nO_{3n+1}$) with a layered cubic perovskite structure. It is isostructural with $La_2CuO_4$, a correlated 3d TMO, which exhibits high $T_c$-superconducting phase when doped with holes.[1,107,108] $Sr_2IrO_4$ shows canted AFM ordering below $T_N \approx 240$ K.[109,110] The naïve band picture expects metallic phase from the odd number of electrons ($5d^5$) in d-orbitals (Figure 5a). However, the optical spectrum of $Sr_2IrO_4$ shows that it is an insulator with a clear optical gap (solid line in Figure 5c). To resolve the controversy, Kim et al. performed a detailed investigation on the electronic structure of $Sr_2IrO_4$ using various tools including ARPES, optical spectroscopy and first-principles calculations.[36]
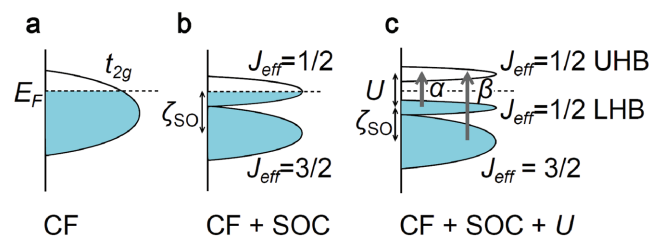
In the study, the crucial role of the SOC and electronic correlation in the MIT mechanism of 5d TM was highlighted.[36] Note that the SOC effect was rarely considered in 3d correlated systems: the energy scale of the SOC constant $\zeta_{SO}$ is $\approx 0.02$ eV, much smaller than $U$ or $W$, and thus was often neglected. The $\zeta_{SO}$ is proportional to $Z^4$ where $Z$ indicates atomic mass and becomes sizable in heavier atoms. It increases to $\approx 0.5$ eV in 5d TM and becomes comparable to $U$ and $W$. Several band calculations had shown the SOC can lead to considerable modification in the electronic structure.[111,112] Nevertheless, the role of large SOC in 5d TM ions had not taken a proper attention before this work.

The essence of the insulating mechanism in $Sr_2IrO_4$ lies in the splitting of $t_{2g}$ states into SOC-induced $J_{eff}$($= L_{eff} + S$) states. In the absence of the SOC, as in the 3d TMOs, the d-orbital states are split into $e_g$ and $t_{2g}$ states under octahedral crystal field ($O_h$ symmetry).[17,113] In such a case, 5 electrons in $Ir^{4+}$ ions of $Sr_2IrO_4$ partially fill the $t_{2g}$ states, resulting in a metallic phase (Figure 5a). Under the strong SOC, however, the $t_{2g}$ states split into effective total angular momentum $J_{eff} = 1/2$ and 3/2 states, the energy separation between them being $\zeta_{SO}$ (Figure 5b). While the $J_{eff} = 3/2$ states are fully filled, $J_{eff} = 1/2$ states are half-filled. One thus still expects a metallic phase. The insulating behavior of $Sr_2IrO_4$ can then be understood under the consideration of $U$. The formation of the narrow $J_{eff} = 1/2$ bands enhances the effect of the Coulomb interaction and opens a Mott gap even with a small value of $U$ (Figure 5c). Therefore, the insulating nature of $Sr_2IrO_4$ originates from the cooperation of the relativistic SOC and the electronic correlation, which opened a new field referred to as the relativistic Mott regime.[36,102,106]

Indeed, the relativistic Mott scheme consistently explains other experimental observations relevant to $Sr_2IrO_4$. Moon et al. observed an insulator to semimetal transition with increasing dimensionality in Ruddlesden–Popper series iridates.[103] The schematic crystal structures of $Sr_{n+1}Ir_nO_{3n+1}$ with $n = 1$ ($Sr_2IrO_4$), 2 ($Sr_3Ir_2O_7$), and $\infty$ ($SrIrO_3$) are shown in **Figure 6**a. In $Sr_2IrO_4$, the plane of $IrO_6$ octahedra are separated by vacuum-like SrO layers, yielding quasi-2D environment on each $IrO_2$ layer. When $n$ is increased to 2 ($Sr_3Ir_2O_7$), two $IrO_2$ layers are stacked in $z$-direction. It becomes completely 3D when $n = \infty$ ($SrIrO_3$).

The optical conductivity spectra of $n = 1, 2,$ and $\infty$ indicate increase in $W$ due to enhanced interlayer coupling. While the $Sr_2IrO_4$ shows clear optical gap of $\approx 0.1$ eV, the gap is much reduced for $Sr_3Ir_2O_7$ and finally vanishes for $SrIrO_3$. Moreover, the redshift in energy position of double peaks is observed with increasing $n$. Note the double peak structure of $\alpha$ and $\beta$ is one of characteristic spectral features found in the iridates; the former is attributed to a transition from lower Hubbard band to upper Hubbard band of the $J_{eff} = 1/2$ while the latter to a transition from $J_{eff} = 3/2$ to UHB (the vertical arrows in Figure 5c).[103,109] The unusually sharp shape of the $\alpha$ peak is a consequence of narrow and parallel $J_{eff} = 1/2$ bands. It is significantly wider in $Sr_3Ir_2O_7$, implying an increase in $W$. It recovers the sharpness in $SrIrO_3$ but the sharpness here originates from the additional tilting of $IrO_6$ octahedron in $SrIrO_3$, not from the dimensionality effect.[114] The increase in $W$ with respect to dimensionality comes from the enhancement in the coupling among $IrO_2$ layers in the $z$-direction. The d bands of neighboring Ir ions hybridize strongly along the $z$-direction, mediated by the apical O ions, which then splits $J_{eff} = 1/2$ bands. The resulting bonding



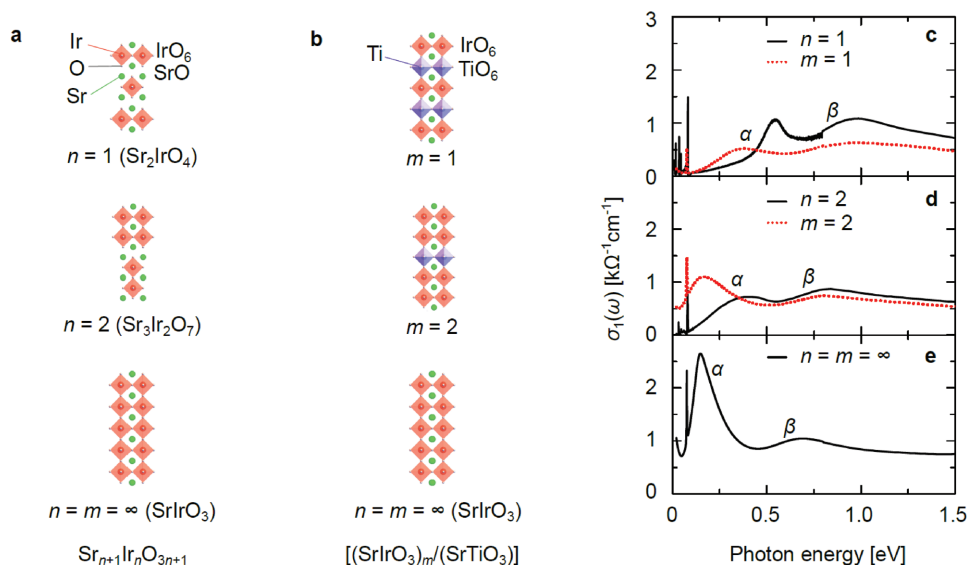**Figure 5.** Schematic energy diagrams for the $5d^5$ configuration of $Sr_2IrO_4$ a) with crystal field (CF) but without SOC and $U$, b) with CF and SOC but without $U$, and c) with CF, SOC and $U$. The energy splitting between orbital states via electronic correlation and SOC are labeled as $U$ and $\zeta_{SO}$, respectively. The dashed horizontal lines indicate the Fermi energy $E_F$. In (c), optical transitions ($\alpha$ and $\beta$) are shown in thick arrows.

**Figure 6.** a–c) Side view of the crystal structure of: a) Ruddlesden–Popper series $Sr_{n+1}Ir_nO_{3n+1}$ and b) [$(SrIrO_3)_m/(SrTiO_3)$] superlattice iridates for $n = m = 1$, $n = m = 2$, and $n = m = \infty$. Sr atoms are shown in green, O atoms in white, Ir atoms in red, and Ti atoms in blue. c–e) The real part of optical conductivity $\sigma_1(\omega)$ for c) $Sr_2IrO_4$ ($n = 1$) at 25 K and $m = 1$ superlattice, d) $Sr_3Ir_2O_7$ ($n = 2$, 10 K) and $m = 2$ superlattice (20 K), and e) $SrIrO_3$ ($n = m = \infty$, 20 K). Sharp peaks observed at energy lower than $\approx 0.1$ eV are IR-active phonons. a,b) Adapted with permission.[117] Copyright 2016, American Physical Society. c–e) Spectra for $n = 1$, 2, and $\infty$: adapted with permission.[113] Copyright 2008, American Physical Society. Spectra for $m = 1$, 2, and $\infty$: adapted with permission.[117] Copyright 2016, American Physical Society.

and antibonding states of the split bands lead to an increase in $W$, resulting in the bandwidth-controlled MIT in $Sr_{n+1}Ir_nO_{3n+1}$.

### 4.3.3. Control of Electronic Correlation in Iridate Heterostructures

Based on electronic structure study results on bulk iridates, modulation of important electronic parameters such $U$ and $W$ was realized in thin films. It was shown that the lattice strain can affect the electronic structure of $Sr_2IrO_4$ thin films grown epitaxially on various substrates.[115] The substrate dependent compressive/tensile strain on $Sr_2IrO_4$ thin films can change the in-plane lattice constants, and consequently the Ir−O−Ir bond angle which affects $W$. Furthermore, they obtained unexpected peak shift in $\alpha$ and $\beta$. This suggests not only $W$ but also $U$ can be modulated by the lattice strain. They also demonstrated that the out-of-plane lattice constant change which affects the apical Ir−O bond length or interlayer coupling cannot be neglected in describing the electronic structure of $Sr_2IrO_4$. The lattice strain thus provides a realistic means to fine-tune $W$ and $U$ in a system with the SOC and $U$.

Modulation of the effective electron correlation was also observed in [$(SrIrO_3)_m/(SrTiO_3)$] superlattice thin films,[116] where importance of lattice geometry was identified.[117] Using the artificial superlattice thin films fabricated via the pulsed laser deposition technique, the dimensionality of $IrO_2$ sheets was systematically increased as shown in Figure 6b.[116] While the $IrO_2$ sheets in Ruddlesden–Popper series iridate compounds are separated by vacuum-like SrO layers, they are separated by insulating $TiO_2$ ($3d^0$) sheets in the [$(SrIrO_3)_m/(SrTiO_3)$] superlattice. Unlike Ruddlesden–Popper series iridates, the Ir and Ti atomic positions are aligned along the same vertical lines in the superlattice thin films. Because the $Sr_{n+1}Ir_nO_{3n+1}$

compounds with $n = 3$, 4, 5, ... are highly unstable in nature, such artificial heterostructures provide a platform for systematic study on the dimensionality effect.[116]

Optical conductivity spectra of the Ruddlesden–Popper series and superlattice iridates are compared in Figure 6c–e. Upon increasing $m$, the number of low-energy carriers increased (exhibiting insulator-like to metallic transition) and the characteristic two-peak structures redshifted in [$(SrIrO_3)_m/(SrTiO_3)$] superlattices. Such a behavior is similar to the evolution of $\sigma_1(\omega)$ from the Ruddlesden–Popper series with increasing $n$. However, a comparison between dimensional counterparts ($n = m$) of the superlattice and Ruddlesden–Popper series iridates revealed an important difference; the $\alpha$ peak is located at a lower energy in the superlattice case. This observation points to the fact that $U$ is reduced in the superlattice iridates.

Optical and first-principles calculations study on superlattice iridates demonstrated that additional hopping paths are mediated by $TiO_2$ blocking layers which should enhance the *in-plane* interactions of Ir ions.[117] We note here the bandgap of $SrTiO_3$ ($3d^0$) is $\approx 3$ eV, much larger than the typical energy scale of $U$ in iridates (0.5 eV). Because of this large gap, the $TiO_2$ layer in the superlattice iridates was regarded as merely a blocking layer that separate $m$-stacks of $IrO_2$ sheets.[116] Indeed, in the band calculation result of the superlattices, Ti $3d$-states were found to be far away from $E_F$ and unlikely to be directly involved in the optical transition for $\alpha$. However, the Ir $t_{2g}$-band dispersion along $M$–$\Gamma$ which is associated with the in-plane hopping between Ir ions was found to be enhanced.[117] The enhancement is due to additional hopping path for Ir ions through Ti ions which share the same apical O ions. These findings lead to conclusion that the change in the lattice geometry can also modulate $W$ and $U$ while the basic electronic structures of Ruddlesden–Popper iridates remain intact.

The studies on $Sr_2IrO_4$ thin films[115] and [$(SrIrO_3)_m$/$(SrTiO_3)$][116,117] demonstrate that fine tuning of electronic structure can be achieved for iridate heterostructures. We note the magnetic structures of iridates can also be very susceptible to lattice parameters.[114,116,118,119] The susceptible nature of the electronic response indicates that iridate and other 5d TM compounds are located near the MIT boundary and are very sensitive to the lattice environment. The control of $U$ and $W$ via lattice modulation is therefore an effective way to design MIT properties of 5d TM compounds.

### 4.3.4. Possible Superconducting Phase in Doped $Sr_2IrO_4$

We briefly discuss the possibility for superconductivity in $Sr_2IrO_4$. $Sr_2IrO_4$ shares common electronic and magnetic states, a (pseudo) spin 1/2 AFM Mott insulator, with the parent compounds of high-$T_c$ cuprates.[36] Based on the similarity, Wang and Senthil proposed the possibility for unconventional superconductivity in electron-doped $Sr_2IrO_4$.[120] Subsequent theoretical studies also point to possible high-$T_c$ superconductivity upon carrier doping; d- and p-wave pairing can be formed by the $J_{eff} = 1/2$ Kramers doublet in electron- and hole-doped $Sr_2IrO_4$, respectively.[121,122]

Naturally, experimental investigations have been made to look for high-$T_c$ superconductivity in doped $Sr_2IrO_4$ by using various techniques including ARPES. A number of ARPES experiments on electron- or hole-doped $Sr_2IrO_4$ reported on the electronic pseudogap.[123,124] Kim et al. have also found in their ARPES study of surface-electron-doped $Sr_2IrO_4$ that the pseudogap represented by a Fermi arc evolves into a d-wave gap at low temperatures.[38] Scanning tunneling spectroscopy measurements of doped $Sr_2IrO_4$ also observed the pseudogap and the d-wave gap.[125,126] An observation of an odd-parity order in the pseudogap phase[127] further strengthens the analogy between iridates and cuprates. Studies on iridates might provide a hint on the longstanding problem of condensed matter physics, i.e., the origin of the pseudogap and the high-$T_c$ superconductivity mechanism. We finally stress that the rich and complex phenomena observed in iridates demonstrate the importance of correlated electronic systems with large SOC as an excellent playground to investigate and control the novel MIT phenomena.

## 4.4. All-In-all-Out 5d Pyrochlore Oxides

### 4.4.1. Magnetism and Metal–Insulator Transition in 5d Pyrochlore Oxides

In regards to the MIT mechanism in TM compounds, we need to understand how the magnetism is coupled to the transition. MITs in 5d pyrochlore $A_2B_2O_7$ (B = Ir, Os) have recently received much attention due to a strong correlation to their ground state with a peculiar AIAO magnetic order.[128–132,201] In this unconventional AFM ground state, all spins of one transition-metal tetrahedron align inward while the others of the neighboring tetrahedra align outward (**Figure 7**a). This AIAO magnetic ordering prompts MITs, and associated exotic quantum phases such as Weyl semimetal[41,42,133,134] and quantum criticality[135] are theoretically predicted to occur. Since the AIAO magnetic ordering preserves the unit cell of pyrochlores, as is the case for $NiS_2$, such MITs should be distinct from the conventional Slater-type MIT. Therefore, a new paradigm is required to understand the MITs and associated novel phenomena.

$Cd_2Os_2O_7$ is a prototypical system with an MIT driven by the AIAO ordering. In this compound, a continuous MIT has been observed at the AFM ordering temperature, $T_N = 227$ K.[136,137] Until the unusual AIAO ordering was known to occur, the MIT in $Cd_2Os_2O_7$ was believed to be a Slater-type transition.[138] However, resonant X-ray scattering and magnetic micro-diffraction studies[137,139] revealed the AIAO magnetic ordering in $Cd_2Os_2O_7$, thereby questioning the proposed Slater-type MIT. Moreover, recent theoretical results are consistent with these experimental observations and predicted a Lifshitz-type MIT for which continuous shifts of electronic bands make FSs disappear.[140,141]

Based on the result from optical spectroscopy study, it was argued that the MIT in $Cd_2Os_2O_7$ should be the Lifshitz-type MIT,[39] in which band shifts occur in a way that the density of states at the Fermi level disappears and results in an MIT. The optical spectroscopy result showed how the AIAO ordering and electronic band structures evolve together in the MIT process. Figure 7b illustrates a simplified schematic diagram for the proposed Lifshitz transition in $Cd_2Os_2O_7$. At high temperatures, electron and hole bands both cross the Fermi level, resulting in a semi-metallic state. As the AIAO order arises, these bands shift away from the Fermi level, gradually reducing the Fermi surface sizes. The main difference between the Slater- and Lifshitz-type
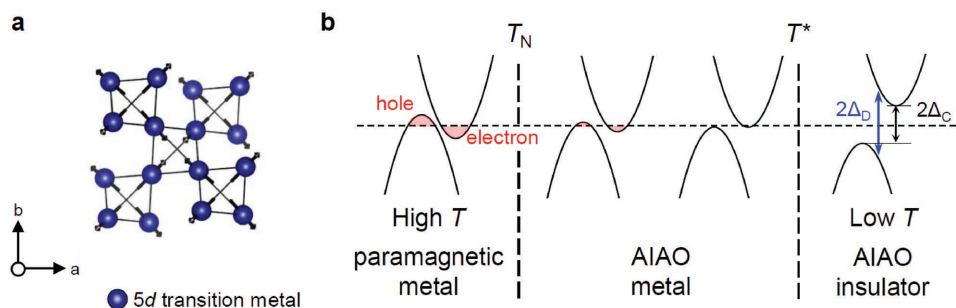


**Figure 7.** a) Simplified schematic view of the AIAO magnetic ordering in 5d pyrochlore. b) Band structure of Lifshitz-type MIT with the AIAO magnetic phase transition. The AIAO ordering forms at $T_N$ in the metal state. In addition, continuous shifts of the electronic bands due to the magnetic ordering additionally induce the AIAO insulating phase below $T^*$. b) Adapted with permission.[39] Copyright 2015, American Physical Society.
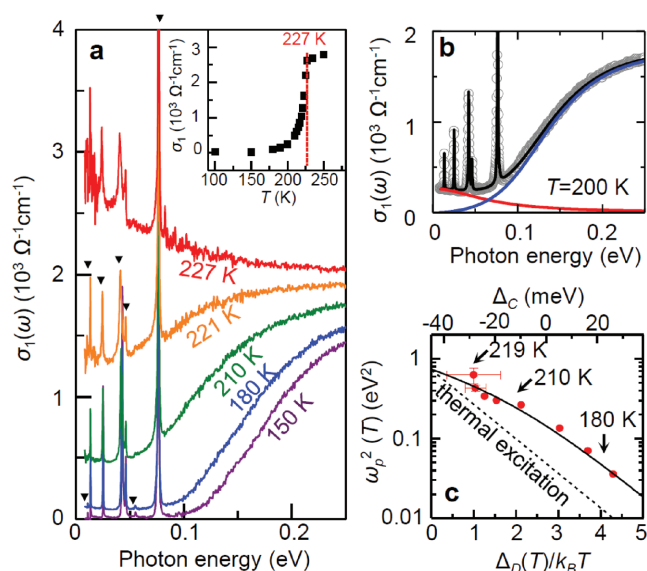
**Figure 8.** a) Temperature-dependent optical conductivity $\sigma_1(\omega)$ from $Cd_2Os_2O_7$ for $\hbar\omega < 0.25$ eV. The solid triangles indicate the IR-active phonons. The inset shows temperature-dependent $\sigma_1(\omega)$ at $\hbar\omega = 20$ meV. b) $\sigma_1(\omega)$ at 200 K with a fit using the model described in the main text. The red (blue) line corresponds to the Drude (CPM0) models and the black line corresponds to the phonons. c) $\omega_p^2(T)$ as a function of $\Delta_D(T)/k_BT$ with the fit expected from the Lifshitz-type band evolution. The dashed line indicates the exponential behavior expected from thermally induced carriers. Adapted with permission.[39] Copyright 2015, American Physical Society.

MITs is the presence of the intermediate AIAO metallic phase. While a finite bandgap should form at $T_N$ for the Slater-type MIT, the intermediate AIAO metallic phase is inevitable from its continuous nature in the case of the Lifshitz-type MIT. The optical study captured this intermediate AIAO metallic state, clarifying the Lifshitz character of the MIT in $Cd_2Os_2O_7$.

The real part of optical conductivity $\sigma_1(\omega)$ from $Cd_2Os_2O_7$ shows the strong coupling between the MIT and the AIAO ordering. **Figure 8**a shows the temperature dependent $\sigma_1(\omega)$ below 0.25 eV. A clear bandgap feature without any spectral weight below the gap at $T < 150$ K indicates an insulating phase. The sharp peaks below the gap correspond to seven infrared active phonons of pyrochlore structures.[142] The phonon frequencies show unusually large $T$-dependent shift, indicating strong spin-phonon coupling in $Cd_2Os_2O_7$.[40] As $T$ increases, the spectral weight in the low energy region shows development of the Drude response from the conducting carriers. To visualize the $T$-dependence of the Drude response, $\sigma_1(\omega)$ at $\hbar\omega = 20$ meV is plotted as a function of $T$ in the inset of Figure 8a. The optical conductivity increases abruptly near $T_N$ (i.e. 227 K), indicating the strong correlation between the MIT and the AIAO ordering.

The detailed $T$-dependent evolution of the optical spectra also implies the existence of the AIAO metallic phase in $Cd_2Os_2O_7$. As shown in Figure 8b, the optical spectra have contributions from infrared-active phonons (black), direct bandgap transition (red) and Drude components by free carriers (blue). Particularly, the $T$-dependent plasma frequency $\omega_p^2(T)$ extracted from the Drude component does not follow the exponential behavior expected from thermal excitations at around $T_N = 227$ K, as can

be seen in Figure 8c. This clearly indicates that the optical gap should continually change as expected in the case of Lifshitz-type MIT. Consequently, the Fermi surface volume also changes continually, which is consistent with the observed $T$-dependent spectral evolution near the AIAO transition. More detailed fittings indicate an existence of a metallic state between $T^* \sim 210$ K and $T_N$, i.e. the AIAO metallic phase (Figure 7b).[39]

### 4.4.2. Control of the Lifshitz-Type MIT in 5d Pyrochlore Oxides

The observed Lifshitz-type transition in $Cd_2Os_2O_7$ can be a general mechanism for MITs found in other 5d pyrochlore oxides, such as iridates. Traditionally, metallic, semimetallic, and topological insulating phases of rare earth pyrochlore iridates have been predicted for a small $U$.[42] As $U$ increases, the two-step transitions should occur from nonmagnetic metal to the AIAO metal and to the AIAO insulator phases, similar to the case of $Cd_2Os_2O_7$. Therefore, the Lifshitz-type MIT mechanism in $Cd_2Os_2O_7$ may work well in the other 5d pyrochlore compounds, in spite of the differences in electronic and magnetic Hamiltonians between iridate and osmate systems.

The MIT in the AIAO pyrochlore driven by the continuous band shifts provides a new route to the control of the transition. Recently, it has been suggested that a correlated phase of Weyl semimetal which has low energy excitations of Weyl fermion with a topological nature may be used as a functional platform for spintronics, considering its nature of topologically protected charges.[143] In particular, the phase can be realized even under symmetry-broken environment. Several theoretical studies predicted that a Weyl semimetal phase should exist in AIAO metallic phases of iridates.[41,42] Therefore, it is highly desired to find such novel phases in iridates by electronic band tuning or external magnetic field. The Lifshitz-type band shift can tune the electronic structure and thus can induce a phase transition between the Weyl and insulating phases.[42] These approaches to control the AIAO magnetic transition can also provide an added benefit of tuning the MIT properties.

### 4.5. The Emergence of Exotic Patterns through Metal–Insulator Transition

When a certain material undergoes an MIT, more often than not a new structure pattern emerges that did not exist before. The MIT found in $Tl_2Ru_2O_7$ is a case in point.[144] At the MIT, it undergoes a spontaneous dimensional lowering and transforms an otherwise 3D cubic lattice of Ru to a 1D chain of Ru orbital, which is likely to follow the physics of Haldane 1D chain with an integer spin.[145,146] Here, enhanced quantum fluctuations drive novel phases in interacting quantum spins when the dimensionality is reduced. In the 1D Heisenberg antiferromagnet the ground state with integer spins is separated from all excited states by a finite spin (Haldane) gap. Needless to say, understanding how the new pattern emerges is directly related to the origin and mechanism of the MIT under question. If the metal–insulator transition is accompanied by a strong SOC, this question can be far more interesting and, at the same time, probably a lot more difficult to solve. Here

**ADVANCED
SCIENCE NEWS**

www.advancedsciencenews.com

**ADVANCED
MATERIALS**

www.advmat.de

we would like to take two examples of such and illustrate how certain interesting patterns emerge in layered materials 1T-TaS$_2$ and Li$_2$RuO$_3$. We also address how emergence of such pattern is related to the MIT.

### 4.5.1. David-Star Pattern of 1T-TaS$_2$

The el–el and el–ph interactions are believed to be responsible for the MIT in 1T-TaS$_2$. 1T-TaS$_2$ exhibits the MIT after a series of first-order (in)commensurate charge-density-wave (CDW) phase transitions. The exotic result of these successive transitions is that new lattice distortions with a pattern of David stars emerge out of the triangular lattice in the high-temperature phase; strong el–el interaction further localizes these electrons, and leads to an insulating ground state.[147,188] Recently, a hidden quantum state was discovered in 1T-TaS$_2$ at temperatures below MIT induced by a ultrafast laser pulse.[148] In the new low-temperature pattern, 12 out of 13 Ta$^{4+}$ 5d-electrons form molecular orbitals in hexagonal star-of-David patterns (**Figure 9**a). This then leaves one 5d-electron providing $S = 1/2$ "orphan" spin with a large spin–orbit interaction in the low-temperature commensurate CDW phase.

Diamagnetic character of the magnetic susceptibility $\chi(T)$ of 1T-TaS$_2$ is interrupted by two jumps signaling corresponding CDW transitions and by a strong paramagnetic Curie–Weiss tail below ≈50 K, suggesting the emergence of short-range correlations at low temperatures as shown by Kratochvilova et al.[149] The effective magnetic moment $\mu_{eff}$ ≈0.08 $\mu_B$/f.u. is roughly half of the expected moment $g_s\sqrt{S(S+1)/13}\,\mu_B$ ≈0.13 $\mu_B$ for $S = 1/2$ per each David star. The Curie–Weiss temperature $\theta_{CW}$ is estimated to be ≈0.02 K, indicating weak low-temperature magnetic correlations. Consistent with $\chi(T)$, the specific heat reveals a sharp drop at ≈50 K. A broad hump in the magnetic heat capacity also suggests some kind of short-ranged order. Using the coefficient $\gamma$ from the specific heat and the low-temperature value of magnetic susceptibility $\chi_0$, we can calculate the Sommerfeld–Wilson ratio as $R_W = \frac{4\pi^2 k_B^2}{3(g\mu B)^2}\frac{\chi_0}{\gamma}$ ≈2, indicating the presence of considerable electronic correlations. This then makes 1T-TaS$_2$ a rare example of MIT with a quantum spin and a strong spin–orbit coupling.

As the bulk measurements showed clear evidences for a low-temperature correlated phase, neutron scattering and $\mu$SR techniques were used provide a better insight into the ground state of 1T-TaS$_2$ as shown by Kratochvilova et al.[149] The $\mu$SR technique is based on the implantation of spin-polarized muons in matter and on the detection of their spin motion affected by the magnetic field, providing information on its local environment and probing the system on a unique timescale. Muons are very sensitive probes of magnetic systems, often can detect effects that are too weak to be seen by other methods; as well as allowing both static and dynamic magnetic behavior to be investigated. The temperature evolution of the initial asymmetry and relaxation rate obtained by $\mu$SR in 1T-TaS$_2$ reveals a change of slope below ≈50 K, corresponding to the abrupt changes in the temperature evolution of specific heat and magnetic susceptibility. To describe the data theoretically, it
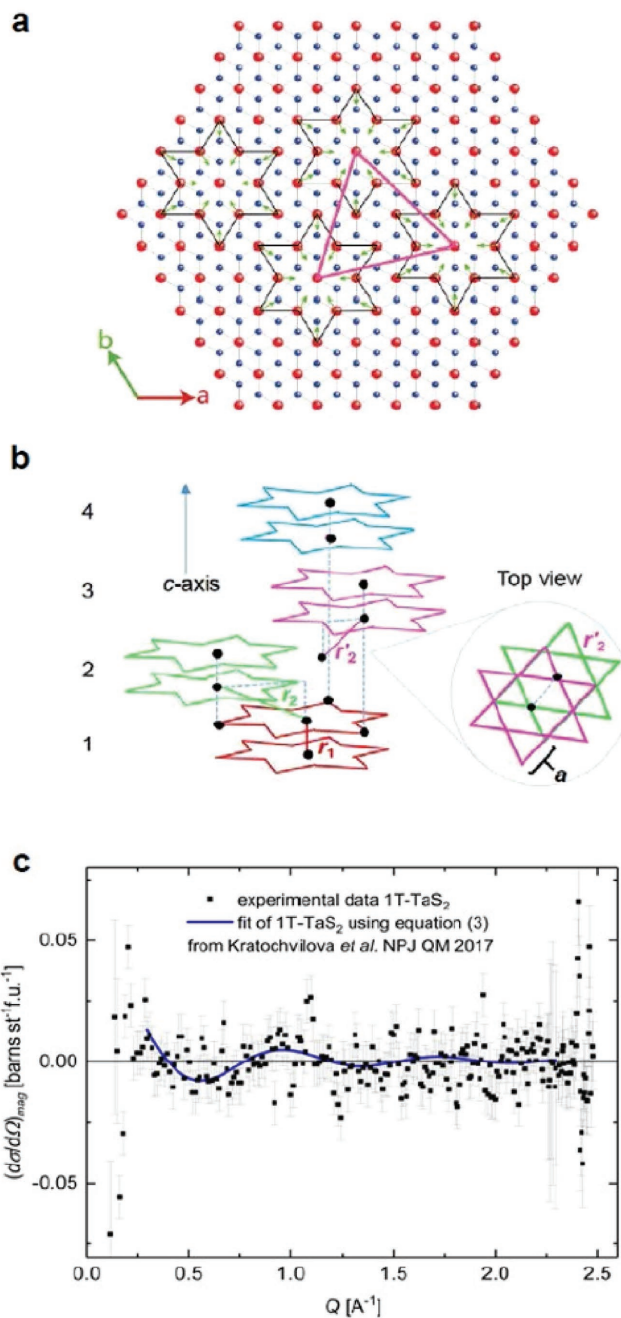


**Figure 9.** a) The monolayer 1T-TaS$_2$ viewed along the $c$-axis. Black line indicates the representative David-star clusters, where in-plane Ta atom displacements are marked by green arrows. The triangular superlattice marked by magenta line is composed of the David-star clusters.[188] b) CDW structure and interplane stacking in 1T-TaS$_2$. The lattice parameter $a = 3.36$ Å is depicted in the top view. In the case of the repetitive stacking with the nearest-neighbor distances $r_1 = 5.90$ Å and $r_2 = 8.29$ Å only double layers 1 and 2 alternate while the screw stacking with the nearest-neighbor distances $r_1$ and $r'_2 = 6.79$ Å is formed by double layers 1 to 4.[149] c) The magnetic scattering cross section of 1T-TaS$_2$ at 1.5 K. The blue line represents the fit described in ref. [149]. Vertical error bars represent $1\sigma$ s.d. counting statistics. Adapted with permission.[149] Copyright 2017, Nature Publishing Group.

is necessary for us to take into account the complex crystal structure of the commensurate CDW phase; the hexagonal sheets form double layers connected by the *c*-stacking vector (Figure 9b). The low-temperature phase is commensurate only in the basal plane because the stacking order established along the *c*-axis is not periodic. Two types of stacking patterns along the *c*-axis—screw and repetitive—have been observed in the ratio $\approx 1{:}2.7$.[150] Figure 9c shows the diffuse magnetic scattering data with a broad hump centered at $Q \approx 0.9$ Å$^{-1}$. Due to the large spatial extent of the David star pattern, the nearest neighbors that are expected to contribute to the magnetic cross section are located across the hexagonal layers and not within them. Indeed, assuming the crucial correlations lying only within the CDW layer, the magnetic scattering data cannot be described satisfactorily. The 3D character of the electronic correlations should be considered in the fit (blue line in Figure 9c) to explain the experimental results.[151–153] Interestingly, the second-nearest neighbor correlations $r_2$ and $r_2'$ are ferromagnetic, corresponding to the positive value of $\theta_{CW}$. The obtained effective magnetic moment of $\approx 0.4\ \mu_B$ represents the upper limit value of the magnetic moment per David star. The $Q$-position



**Figure 10.** a) The crystal structure of Li$_2$RuO$_3$ above the MIT temperature (Ru atoms are shown in gray, Li atoms in green, and O atoms in red). b) Resistivity (marked by red line) and magnetic susceptibility (marked by blue line) as a function of temperature. c) Theoretically predicted orbital pattern Red lines mark dimerized bonds and black lines mark the extended ones. The dimerized bonds form the herringbone structure, which seems to play a crucial role in the formation of the valence bond crystal state. d) Low-temperature powder X-ray diffraction pattern with the superlattice peak shown in the inset.

implies ferromagnetic correlations between pairs of spins across the hexagonal layers. To sum up, commensurate lattice modulation in 1T-TaS$_2$ is accompanied by electronic reconstructions, leaving exactly one conduction electron per David-star. Strong electron interaction localizes these electrons, and leads to an insulating ground state. Deep in this Mott insulating state, a highly correlated phase was discovered.

### 4.5.2. Herringbone Pattern of Li$_2$RuO$_3$

Li$_2$RuO$_3$ reveals a regular honeycomb lattice of edge-sharing RuO$_6$-octahedra as shown in **Figure 10**a. The compound undergoes a structural phase transition into a Mott-insulating state at $\approx 550$ K from $C2/m$ to $P2_1/m$.[154] In this new type of pattern, the honeycomb lattice is drastically distorted. The orbital degree of freedom and strong spin–orbit physics form the ground state into a nonmagnetic dimerized superstructure. What is intriguing is that below the MIT one third of Ru−Ru bonds shorten significantly and this structural phase transition leads to singlet dimer formation in a herringbone fashion out of the regular honeycomb lattice.[154]

The phase transition is illustrated by a sudden increase in the resistivity and, at the same time, the magnetic susceptibility drops to $\approx 10^{-4}$ emu mol$^{-1}$ below the MIT (Figure 10b). For example, inter Ru$^{4+}$ ion bonds in the 2D plane of regular honeycomb lattice have similar lengths about 2.9 Å in the high-temperature phase, but one third of the bonds are shortened below the transition temperature (Figure 10c). The length
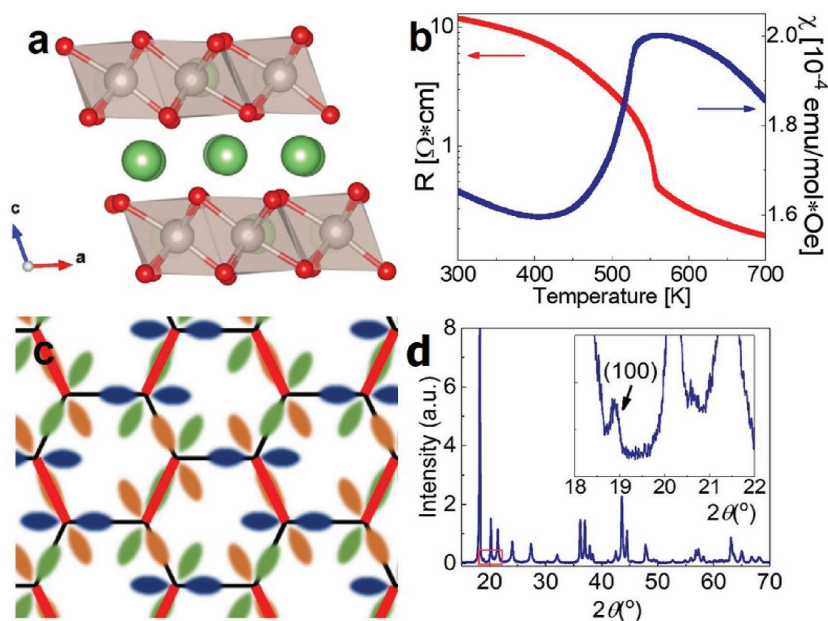
of the dimerized bonds is 2.57 Å while the others are about 3.04 Å. Thus, the ratio between two sets of bonds exceeds 15% at 300 K, which is extremely large for any oxides with an MIT. Moreover, these dimerized bonds form a herringbone pattern where the short bonds in the hexagon do not face each other, as is reflected in the low-temperature powder diffraction (Figure 10d). This kind of pattern has not been found in other related materials with other TM ion such as Li$_2$IrO$_3$. Besides, the huge dimerization and the high transition temperature are unique among materials with similar structures. All these observations at least appear to be consistent with a simple picture of a bandgap opening with a reduction in the density of states. We note that the localized magnetic moment of Ru$^{4+}$ does not order antiferromagnetically.[155] At the same time, the distances between Ru$^{4+}$ and O$^{2-}$ around the TM ion vary, leading to the octahedron distortion. This behavior suggests that this phenomenon is related to the change in the orbitals.[154]

This cooperative Jahn–Teller distortion perturbs the energy levels of t$_{2g}$ orbitals, which are degenerate under cubic crystal fields given by O$^{2-}$ ions. Some of the experimental observations have been explained by band calculations with the $\delta$- and $\pi$-bonds.[154,156] Because of the large energy gap between the $\sigma$- and the other bonds, electron in the $\sigma$-bond has lower effective dimensionality than the honeycomb layer containing the Ru ions.[157] t$_{2g}$ orbitals of Ru$^{4+}$ in $d^4$ cannot form an electronic net or chain; instead, they form dimer "dots." The ground state of orbitals in Li$_2$RuO$_3$ is shown in Figure 10c.[158] Because of the reduced dimensions of the electron motion, an orbital-selective Peierls transition can occur in this system.[157] In

this theoretical scheme, two electrons in the dimerized bond are in a singlet state with $S = 0$. This phenomenon is called a valence bond solid state.[156] Upon this phase transition, distance between dimers increases and the overlap between wave functions of dimers decreases. Therefore, the electron hopping becomes more difficult and as a result, the resistivity increases.

## 5. Application Aspect

In Section 4, we have reviewed results of our studies on various MIT systems. While the main purpose of our investigations was to understand the microscopic mechanisms for the novel MIT phenomena, we wish to discuss, based on what we have discussed in Section 4, potential applications of the MIT materials with their strengths and weaknesses. In addition, we would like to briefly touch upon some of the efforts to overcome these weaknesses.

### 5.1. Potential Applications

The beauty of using functional materials lies in the fact that they exhibit the target functionality, i.e., the material itself is a device. Because the material itself responds to certain stimulus, each material can be used as a sensor or a detector in its simplest form. There are a variety of MIT-inducing trigger mechanisms (e.g., temperature, mechanical pressure, chemical doping, and external electric/magnetic fields) and each one of them can be utilized for a sensor if it is within the operating range. As mentioned earlier, vanadate is already being used in commercial fire detectors, utilizing its sensitivity to the temperature in the right range.[13] As the vanadate example shows, the external parameter that triggers the MIT needs to be accessible. In the following, we discuss potential applications for some of the materials discussed in the previous section.

All the materials that possess MIT properties in principle can be used for switches or logic devices. One of the most convenient and thus desired trigger mechanisms is the electric field or voltage gating which can easily be applied on existing electronic devices. In that context, novel electric devices such as Mott FET (Mott field-effect transistor) and neuromorphic devices utilizing Mott insulator-based ReRAM devices are potential candidates for practical use of correlated materials such as $VO_2$[159–165] and $NiS_{2-x}Se_x$.[164,165] A critical intrinsic weakness for most of the Mott insulators is the low carrier mobility.[162]

Even though not directly utilizing the MIT property, it was recently proposed that 5d TMO pyrochlore, specifically $Nd_2Ir_2O_7$ and $Cd_2Os_2O_7$, could serve as microscopic and electrically readable magnetic medium that can be utilized in domain wall nanoelectronics.[166,167] These materials exhibit the AIAO antiferromagnetic ordering upon which metallic phase undergoes a transition into an insulating state where two kinds of magnetic domains can coexist, namely the AIAO and the all-out/all-in. The domain wall with such antiferromagnetic order shows higher stability than that in ferromagnetic memory devices,[168] which could allow higher-density integration.[167] For practical use of the novel functionality, however, the transition temperature has to be in the operating range.

We have discussed a few examples of potential applications for the MIT materials. In **Table 2**, we list potential applications for the materials we have investigated along with their strengths

**Table 2.** Characteristics of MIT materials relevant to application.

| Material | Trigger(s) for the MIT | Potential applications | Strength | Weakness |
|---|---|---|---|---|
| $VO_2$ | Temperature (340 K) | Fire alarm[13] | Sub-nanosecond time scale switch[190] | Low carrier mobility ($\approx 0.1$ cm$^2$ V$^{-1}$ s$^{-1}$)[162] |
| | Pressure ($\approx 10$ GPa)[189] | Gas sensor[191] | High operating temperature | |
| | $E$-field ($\approx 10^4$–$10^5$ V cm$^{-1}$)[161,190] | Nonvolatile memory device[161] | | |
| | Hydrogenation[191] | Bolometric detector[192,193] | | |
| $NiS_{2-x}Se_x$ | Temperature ($T_C < 90$ K) | Pressure sensor | Low threshold pressure | Low operating temperature |
| | Pressure ($x = 0$: $\approx 3$ GPa[194]; $x \approx 0.4$: $\approx 0.2$ GPa[195]) | Uncooled bolometer[196] | | Large device size |
| | $E$-field ($x = 0.11$: $\approx 4$ kV cm$^{-1}$) | Nonvolatile memory device[164,165] | | High threshold field |
| $Ca_{2-x}M_xRuO_4$ ($M$ = Sr, Ti, Fe) | Temperature ($Ca_2RuO_4$: $\approx 357$ K)[197,198] | Temperature sensor | Low threshold $E$-field | Low operating temperature |
| | $E$-field ($\approx 40$ V cm$^{-1}$)[178] | Bolometric detector[196] | | Damage on the single crystal upon structural transition[178,200] |
| | Pressure ($x = 0$: $\approx 1.5$ GPa)[199] | | | |
| 5d pyrochlore $R_2Ir_2O_7$ ($R$ = Rare earth), $Cd_2Os_2O_7$ | Temperature ($R_2Ir_2O_7$: $\approx 34$–110 K[102,129]; $Cd_2Os_2O_7$: $\approx 227$ K[40]) | Magnetic domain wall race track memory[166,168] | Electronically readable memory storage[166,168] | Low operating temperature[167] |
| | | Domain wall nanoelectronics[167] | Higher-density integration of device[167] | Difficulty in synthesis[201] |

**ADVANCED
SCIENCE NEWS**

www.advancedsciencenews.com

**ADVANCED
MATERIALS**

www.advmat.de

and weaknesses. A variety of potential applications may be found for the materials. In the process, machine learning approaches that are now actively being used in various disciplines may be useful in selecting and/or designing suitable material for device applications.[169,170] While the strengths may be utilized for potential applications, the weaknesses need to be overcome. A most notable weakness of correlated MIT materials is that they have MIT temperatures away from accessible range. The information we gathered through our studies can provide some clues for overcoming such weaknesses as discussed in Section 5.2.

## 5.2. Overcoming Weakness for MIT Application

For the practical use of correlated MIT materials, the operating range for an external parameter should be accessible. For example, the practical use of a material for electronic devices would be difficult if the material has a low MIT temperature. Such weaknesses or limitations need to be overcome for the materials to be used for practical applications by, for example, moving the operating external parameter within the accessible range. The information we obtained through our studies can be useful in determining what to try and even what not to try. An example can be found in the case of bandwidth-controlled MIT in $Sr_{n+1}Ir_nO_{3n+1}$ ($Sr_2IrO_4$, $Sr_3Ir_2O_7$, and $SrIrO_3$), for which the SOC strength plays a critical role in opening the Mott gap as explained in Section 4.3.2.[36,103] As the SOC is an intrinsic property of an atom, it would be difficult to change MIT properties of such materials in general.

In this section, we wish to discuss the methodology to overcome shortcomings of MIT properties in TM compounds for real applications. We have already seen a variety of TM compounds for which MIT properties are affected by external perturbations. Most prominently, structural distortions are critical to MIT phenomena as exemplified by 3d $VO_2$ and 4d $Ca_{2-x}Sr_xRuO_4$ cases as discussed in Section 4. Here, we will present some attempts to control the MIT temperatures by artificial structural distortions as well as chemical doping, strain engineering[189,194,195,199] and E-field (electric-field)[178,190] application. Furthermore, we will briefly introduce recent intriguing results on ultrafast MIT phenomena, where femtosecond optical pulses induce the MIT through photodoping effects or direct phonon perturbation.

### 5.2.1. MIT Control by Structural Modulations

In the microscopic point of view, local lattice structure plays the critical role in the determination of the overall physical properties. In particular, $TMO_6$ octahedral rotation or tilting distortions in perovskite materials can heavily influence the bandwidth $W$, and MIT properties as well. In 3d nickelates, A-site substitution with smaller ions makes the Ni−O−Ni bonding angle increase and thus bandwidth $W$, and the material becomes metallic due to a larger overlap between orbitals.[10,171] In addition to atomic substitution, structural modulation by strain engineering has been intensively performed on nickelate thin films, where a sensitive control of $T_c$ has been obtained by using different substrates.[172,173]

Recently, it was also revealed that hydrogen doping to perovskite nickelates dramatically reduces the carrier density due to a band-filling effect.[174,175] More specifically, the band-filling in $e_g$ orbital blocks the intersite hopping channel upon octahedral distortions. Indeed, in addition to nickelates, other 3d-TM compounds such as manganites[176] and vanadates[10] also show the structural dependence of $T_c$'s.

Another prominent example for structural $T_c$ modulation can be found in 4d-TM $Ca_{2-x}Sr_xRuO_4$. As $Sr_2RuO_4$ is doped with $Ca^{2+}$ ions, an octahedral rotation distortion develops. Subsequently, at the doping of $x = 0.5$, additional tilting distortion arises.[177] An insulating phase suddenly appears at $x = 0.2$, and $T_c$ rises to 357 K at the $x = 0$ compound $Ca_2RuO_4$.[197,198] Application of an external E-field is also found to induce an MIT with lattice distortions.[178] Interestingly, the electric-field-driven metallic state shows the same lattice structure as that of the thermally induced metallic phase.[178,200] Kyung et al. recently studied a similar E-field effect in $Sr_2RuO_4$ and found that a strong external E-field can induce rotation distortions at the surface, and consequently the electronic structures are deformed. The results mentioned above clearly show that precise $T_c$ control may be achieved by doping and strain techniques as well as E-field, all of which can induce lattice distortions.

In contrast to 3d and 4d TM compounds, it is difficult to vary the MIT properties by structural distortions for 5d materials. As we learned from the results discussed in Section 4.3, physical properties of 5d TM compounds are dominated by the SOC and el–el correlation. These properties are of intrinsic nature of an atom and are difficult to change via external stimuli, such as pressure, chemical doping, or electric/magnetic-fields. This fact makes it difficult to control the MIT phenomena in 5d-TM compounds. This is clearly different from the 3d/4d cases for which bandwidth is the key parameter and thus MITs are relatively easily controlled. In other words, electronic phases in 5d compounds seem to be more stable.

### 5.2.2. Ultrafast Photoinduced MIT

One of the most promising methods to control the MIT is photodoping by ultrafast optical pulses. Extensive and intensive studies have been recently performed on the photoinduced MIT (PI-MIT) phenomena. Femtosecond light pulses induce insulator-to-metal transition in TM compounds such as manganites and vanadates. Triggering MIT by femtosecond pulses has advantages for application due to its extremely short switching time scale and noncontact process. Here, we present a brief introduction to ultrafast pump–probe spectroscopy for investigation of the photoinduced MIT. In addition, several specific examples of PI-MITs in TM compounds are discussed.

Ultrafast spectroscopy is an emerging tool for investigation of quantum interactions in TM compounds. Excitations by femtosecond pulses can induce macroscopic phase transitions, such as melting of magnetic/charge ordered states and insulator–metal transitions.[160,179] In addition, tracing real-time responses by the technique can identify interactions between different degrees of freedom through inspection of the recovery process back to the equilibrium state.[180,181] For the ultrafast technique,
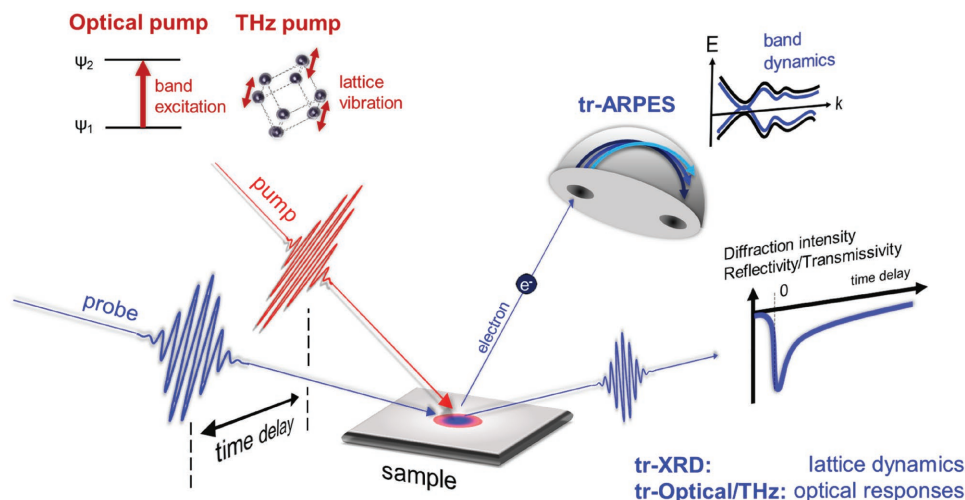
**Figure 11.** Schematic diagram of various pump–probe spectroscopy techniques. In this ultrafast technique, the probe beam traces the dynamical response after the system is excited by the pump beam. As the pumping source, optical and THz beams can be used to generate photoinduced charges or phonon excitations. As for the probe beam, X-rays and optical/THz beams can be used to investigate ultrafast lattice dynamics and optical responses. Investigation of electronic band response is also possible by using femtosecond UV light in ARPES.

various light sources are employed to target the interaction of interest. **Figure 11** shows a schematic diagram of ultrafast techniques—pump–probe spectroscopy—where the probe beam traces the dynamical response after the system is excited by the pump beam. Optical as well as THz beams have been widely utilized as the ultrashort pump source to have photoinduced charges across the insulating gap or phonon excitations (lattice perturbation). As for the probe beam, X-rays and optical/THz pulses can be used to investigate ultrafast lattice dynamics and optical responses. If one uses femtosecond UV light in ARPES, investigation of electronic band response is also possible.

The most popular TM materials for photoinduced MIT study are vanadates. As discussed earlier, vanadates such as $VO_2$ and $V_2O_3$ are recognized as canonical Mott–Hubbard systems, where electron correlation plays a crucial role in inducing the MIT. A variety of ultrafast studies with optical and THz pulses have been performed to obtain dynamics involved in anomalous photoinduced MIT in vanadates. In $VO_2$, near-infrared optical pumping induces an insulator-to-metal transition with ultrafast changes in the optical response[182,183] and structural distortion.[182] Specifically, the transition is mainly driven by the electronic correlation between photoinduced carriers from optical transitions across the optical gap. $V_2O_3$ also features the PI-MIT with optical pumping, in which insulator-to-metal transition is also accompanied by antiferromagnetic to paramagnetic phase transition.[184] These results indicate that the optical pumping can also be utilized to tune magnetic properties accompanying the MIT.

Manganite is another intriguing platform for the PI-MIT. Very interestingly, THz pumping also induces insulator-to-metal transition in $Pr_{1-x}Ca_xMnO_3$, especially when the photon energy is in resonance with a specific phonon vibration mode along the Mn—O bond.[185] This phonon vibration directly influences orbital interaction through the Mn—O—Mn bonding channel which can perturb the electronic bandwidth and induce ultrafast MIT switching. This evidently shows that ultrafast phonon perturbation can be a controlling factor for MIT switching. In

insulating $Pr_{0.55}(Ca_{1-y}Sr_y)_{0.45}MnO_3$, femtosecond optical pulse changes the system into a metallic phase that does not exist in equilibrium conditions.[186] This photoinduced conducting phase is fairly stable even after pumping pulse has left the sample. A subsequent reversing process back to the insulating phase is also possible with continuous lasing irradiation through heating effect. This is an example of optical switching utilizing MIT. In addition to aforementioned vanadates and manganites, another TM compound comes into the picture and makes the PI-MIT more important; a TM dichalcogenide 1T-TaS$_2$[148] features a hidden metallic phase with ultrafast optical pumping.

## Conflict of Interest

The authors declare no conflict of interest.

## Keywords

**ADVANCED
SCIENCE NEWS**

www.advancedsciencenews.com

**ADVANCED
MATERIALS**

www.advmat.de

[1] P. W. Anderson, *Science* **1987**, *235*, 1196.

[2] A. Damascelli, Z. Hussain, Z. X. Shen, *Rev. Mod. Phys.* **2003**, *75*, 473.

[3] J. D. Jorgensen, B. Babrowski, S. Pei, D. G. Hinks, L. Soderhold, B. Morosin, J. E. Schirber, E. L. Venturini, D. S. Ginley, *Phys. Rev. B* **1988**, *38*, 11337.

[4] Y. Tokura, *Rep. Prog. Phys.* **2006**, *69*, 797.

[5] A. P. Ramirez, *J. Phys.: Condens. Matter* **1997**, *9*, 8171.

[6] S. Y. Jang, D. Lee, J. H. Lee, T. W. Noh, Y. Jo, M. H. Jung, J. S. Chung, *Appl. Phys. Lett.* **2008**, *93*, 162507.

[7] W. S. Choi, S. J. Moon, S. S. A. Seo, D. Lee, J. H. Lee, P. Murugavel, T. W. Noh, Y. S. Lee, *Phys. Rev. B* **2008**, *78*, 054440.

[8] W. S. Choi, D. G. Kim, S. G. A. Seo, S. J. Moon, D. Lee, J. H. Lee, H. S. Lee, D. Y. Cho, Y. S. Lee, P. Murugavel, J. Yu, T. W. Noh, *Phys. Rev. B* **2008**, *77*, 045137.

[9] N. F. Mott, *Rev. Mod. Phys.* **1968**, *40*, 677.

[10] M. Imada, A. Fujimori, Y. Tokura, *Rev. Mod. Phys.* **1998**, *70*, 1039.

[11] J. H. de Boer, E. J. W. Verwey, *Proc. Phys. Soc.* **1937**, *49*, 59.

[12] F. Walz, *J. Phys.: Condens. Matter* **2002**, *14*, R285.

[13] J. Verkelis, Z. Bliznikas, K. Breive, V. Dikinis, R. Sarmaitis, *Sens. Actuators, A* **1998**, *68*, 338.

[14] B. J. Kim, Y. W. Lee, B. G. Chae, S. J. Yun, S. Y. Oh, H. T. Kim, Y. S. Lim, *Appl. Phys. Lett.* **2007**, *90*, 023515.

[15] H. T. Kim, B. Kim, J. C. Park, *US9660190 B2*, **2017**.

[16] M. Nakano, K. Shibuya, D. Okuyama, T. Hatano, S. Ono, M. Kawasaki, Y. Iwasa, Y. Tokura, *Nature* **2012**, *487*, 459.

[17] D. Khomskii, *Transition Metal Compounds*, Cambridge University Press, Cambridge, UK **2014**.

[18] J. C. Slater, *Phys. Rev.* **1951**, *82*, 538.

[19] V. Heine, L. F. Mattheiss, *J. Phys. C: Solid State Phys.* **1971**, *4*, L191.

[20] K. Terakura, A. R. Williams, T. Oguchi, J. Kübler, *Phys. Rev. Lett.* **1984**, *52*, 1830.

[21] R. D. Averitt, A. J. Taylor, *J. Phys.: Condens. Matter* **2002**, *14*, R1357.

[22] C. Kittel, *Introduction to Solid State Physics*, Wiley, Hoboken, NJ, USA **2005**.

[23] P. W. Anderson, *Phys. Rev.* **1958**, *109*, 1492.

[24] F. Evers, A. D. Mirlin, *Rev. Mod. Phys.* **2008**, *80*, 1355.

[25] P. A. Lee, D. S. Fisher, *Phys. Rev. Lett.* **1981**, *47*, 882.

[26] L. D. Landau, S. I. Pekar, *Zh. Eksp. Teor. Fiz.* **1948**, *18*, 419.

[27] K. H. Kim, J. H. Jung, T. W. Noh, *Phys. Rev. Lett.* **1998**, *81*, 1517.

[28] M. W. Kim, J. H. Jung, K. H. Kim, H. J. Lee, J. Yu, T. W. Noh, Y. Moritomo, *Phys. Rev. Lett.* **2002**, *89*, 016403.

[29] Z. X. Shen, D. S. Dessau, *Phys. Rep.* **1995**, *253*, 1.

[30] A. Georges, G. Kotliar, W. Krauth, M. Rozenberg, *Rev. Mod. Phys.* **1996**, *68*, 13.

[31] G. Kotliar, S. Y. Savrasov, K. Haule, V. S. Oudovenko, O. Parcollet, C. A. Marianetti, *Rev. Mod. Phys.* **2006**, *78*, 865.

[32] A. Koga, N. Kawakami, T. M. Rice, M. Sigrist, *Phys. Rev. Lett.* **2004**, *92*, 216402.

[33] V. I. Anisimov, I. A. Nekrasov, D. E. Kondakov, T. M. Rice, M. Sigrist, *Eur. Phys. J. B* **2002**, *25*, 191.

[34] J. S. Lee, S. J. Moon, T. W. Noh, S. Nakatsuji, Y. Maeno, *Phys. Rev. Lett.* **2006**, *96*, 57401.

[35] M. Neupane, P. Richard, Z. H. Pan, Y. M. Xu, R. Jin, D. Mandrus, X. Dai, Z. Fang, Z. Wang, H. Ding, *Phys. Rev. Lett.* **2009**, *103*, 097001.

[36] B. J. Kim, H. Jin, S. J. Moon, J.-Y. Kim, B.-G. Park, C. S. Leem, J. Yu, T. W. Noh, C. Kim, S.-J. Oh, J.-H. Park, V. Durairaj, G. Cao, E. Rotenberg, *Phys. Rev. Lett.* **2008**, *101*, 076402.

[37] Y. K. Kim, O. Krupin, J. D. Denlinger, A. Bostwick, E. Rotenberg, Q. Zhao, J. F. Mitchell, J. W. Allen, B. J. Kim, *Science* **2014**, *345*, 187.

[38] Y. K. Kim, N. H. Sung, J. D. Denlinger, B. J. Kim, *Nat. Phys.* **2015**, *12*, 37.

[39] C. H. Sohn, H. Jeong, H. Jin, S. Kim, L. J. Sandilands, H. J. Park, K. W. Kim, S. J. Moon, D.-Y. Cho, J. Yamaura, Z. Hiroi, T. W. Noh, *Phys. Rev. Lett.* **2015**, *115*, 266402.

[40] C. H. Sohn, C. H. Kim, L. J. Sandilands, N. T. M. Hien, S. Y. Kim, H. J. Park, K. W. Kim, S. J. Moon, J. Yamaura, Z. Hiroi, T. W. Noh, *Phys. Rev. Lett.* **2017**, *118*, 117201.

[41] W. Witczak-Krempa, Y. B. Kim, *Phys. Rev. B* **2012**, *85*, 045124.

[42] W. Witczak-Krempa, A. Go, Y. B. Kim, *Phys. Rev. B* **2013**, *87*, 155101.

[43] D. N. Basov, R. D. Averitt, D. van der Marel, M. Dressel, K. Haule, *Rev. Mod. Phys.* **2011**, *83*, 471.

[44] A. Einstein, *Ann. Phys.* **1905**, *332*, 132.

[45] A. Damascelli, *Phys. Scr.* **2003**, *T109*, 61.

[46] M. Yi, Z.-K. Liu, Y. Zhang, R. Yu, J.-X. Zhu, J. J. Lee, R. G. Moore, F. T. Schmitt, W. Li, S. C. Riggs, J.-H. Chu, B. Lv, J. Hu, M. Hashimoto, S.-K. Mo, Z. Hussain, Z. Q. Mao, C. W. Chu, I. R. Fisher, Q. Si, Z.-X. Shen, D. H. Lu, *Nat. Commun.* **2015**, *6*, 7777.

[47] M. Yi, D. H. Lu, R. Yu, S. C. Riggs, J. H. Chu, B. Lv, Z. K. Liu, M. Lu, Y. T. Cui, M. Hashimoto, S. K. Mo, Z. Hussain, C. W. Chu, I. R. Fisher, Q. Si, Z. X. Shen, *Phys. Rev. Lett.* **2013**, *110*, 67003.

[48] I. H. Inoue, I. Hase, Y. Aiura, A. Fujimori, Y. Haruyama, T. Maruyama, Y. Nishihara, *Phys. Rev. Lett.* **1995**, *74*, 2539.

[49] R. O. Jones, *Rev. Mod. Phys.* **2015**, *87*, 897.

[50] I. H. Inoue, *Phys. Rev. B* **1998**, *58*, 4372.

[51] W. F. Brinkman, T. M. Rice, *Phys. Rev. B* **1970**, *2*, 4302.

[52] K. Kadowaki, S. B. Woods, *Solid State Commun.* **1986**, *58*, 507.

[53] M. Fox, *Optical Properties of Solids*, Oxford University Press Inc., New York **2002**.

[54] J. D. Jackson, *Classical Electrodynamics*, John Wiley & Sons Inc., New York **2007**.

[55] M. M. Qazilbash, A. A. Schafgans, K. S. Burch, S. J. Yun, B. G. Chae, B. J. Kim, H. T. Kim, D. N. Basov, *Phys. Rev. B* **2008**, *77*, 115121.

[56] A. V. Puchkov, D. N. Basov, T. Timusk, *J. Phys.: Condens. Matter* **1996**, *8*, 10049.

[57] M. Dressel, G. Gruner, *Electrodynamics of Solids: Optical Properties of Electrons in Matter*, Cambridge University Press, Cambridge, UK **2002**.

[58] Y. S. Lee, K. Segawa, Z. Q. Li, W. J. Padilla, M. Dumm, S. V Dordevic, C. C. Homes, Y. Ando, *Phys. Rev. B* **2005**, *72*, 054529.

[59] D. Van Der Marel, H. J. A. Molegraaf, J. Zaanen, Z. Nussinov, F. Carbone, A. Damascelli, H. Eisaki, M. Greven, P. H. Kes, M. Li, *Nature* **2003**, *425*, 271.

[60] H. C. Choi, B. I. Min, J. H. Shim, K. Haule, G. Kotliar, *Phys. Rev. Lett.* **2012**, *108*, 016402.

[61] M. Fath, S. Freisem, A. A. Menovsky, Y. Tomioka, J. Aarts, J. A. Mydosh, *Science* **1999**, *285*, 1540.

[62] A. S. Mcleod, E. Van Heumen, J. G. Ramirez, S. Wang, T. Saerbeck, S. Guenon, M. Goldflam, *Nat. Phys.* **2016**, *13*, 80.

[63] M. Liu, A. J. Sternbach, M. Wagner, T. V Slusar, T. Kong, S. L. Bud'ko, S. Kittiwatanakul, M. M. Qazilbash, A. McLeod, Z. Fei, E. Abreu, J. Zhang, M. Goldflam, S. Dai, G.-X. Ni, J. Lu, H. A. Bechtel, M. C. Martin, M. B. Raschke, R. D. Averitt, S. A. Wolf, H.-T. Kim, P. C. Canfield, D. N. Basov, *Phys. Rev. B* **2015**, *91*, 245155.

[64] K. Miyano, T. Tanaka, Y. Tomioka, Y. Tokura, *Phys. Rev. Lett.* **1997**, *78*, 4257.

[65] V. R. Morrison, R. P. Chatelain, K. L. Tiwari, A. Hendaoui, A. Bruhács, M. Chaker, B. J. Siwick, *Science* **2014**, *346*, 445.

[66] T. L. Cocker, L. V Titova, S. Fourmaux, G. Holloway, H. Bandulet, D. Brassard, J. Kieffer, M. A. El Khakani, F. A. Hegmann, *Phys. Rev. B* **2012**, *85*, 155120.

[67] B. T. O'Callahan, A. C. Jones, J. Hyung Park, D. H. Cobden, J. M. Atkin, M. B. Raschke, *Nat. Commun.* **2015**, *6*, 6849.

**ADVANCED
SCIENCE NEWS**
www.advancedsciencenews.com

**ADVANCED
MATERIALS**
www.advmat.de

[68] N. F. Mott, R. Peierls, *Proc. Phys. Soc.* **1937**, *49*, 72.

[69] H.-D. Kim, H. Kumigashira, A. Ashihara, T. Takahashi, Y. Ueda, *Phys. Rev. B* **1998**, *57*, 1316.

[70] K. E. Smith, V. E. Henrich, *Phys. Rev. B* **1994**, *50*, 1382.

[71] K. E. Smith, V. E. Henrich, *Phys. Rev. B* **1988**, *38*, 5965.

[72] G. A. Sawatzky, D. Post, *Phys. Rev. B* **1979**, *20*, 1546.

[73] S.-K. Mo, J. D. Denlinger, H.-D. Kim, J.-H. Park, J. W. Allen, A. Sekiyama, A. Yamasaki, K. Kadono, S. Suga, Y. Saitoh, T. Muro, P. Metcalf, G. Keller, K. Held, V. Eyert, V. I. Anisimov, D. Vollhardt, *Phys. Rev. Lett.* **2003**, *90*, 186403.

[74] A. Matsuura, H. Watanabe, C. Kim, S. Doniach, Z.-X. Shen, T. Thio, J. Bennett, *Phys. Rev. B* **1998**, *58*, 3690.

[75] A. Matsuura, Z. Shen, D. Dessau, C. Park, T. Thio, J. Bennett, O. Jepsen, *Phys. Rev. B* **1996**, *53*, R7584.

[76] P. Kwizera, M. Dresselhaus, D. Adler, *Phys. Rev. B* **1980**, *21*, 2328.

[77] H. C. Xu, Y. Zhang, M. Xu, R. Peng, X. P. Shen, V. N. Strocov, M. Shi, M. Kobayashi, T. Schmitt, B. P. Xie, D. L. Feng, *Phys. Rev. Lett.* **2014**, *112*, 087603.

[78] G. Han, B. G. Jang, Y. Y. Koh, J. J. Seo, S. Soltani, Y. K. Kim, W. S. Kyung, C. M. Cheng, K. D. Tsuei, K. D. Lee, N. Hur, H. Kim, J. H. Shim, C. Kim, unpublished.

[79] S. A. Carter, T. F. Rosenbaum, P. Metcalf, J. M. Honig, J. Spalek, *Phys. Rev. B* **1993**, *48*, R16841.

[80] M. Matsuura, H. Hiraka, K. Yamada, Y. Endoh, *J. Phys. Soc. Jpn.* **2000**, *69*, 1503.

[81] F. Gautier, G. Krill, M. F. Lapierre, P. Panissod, C. Robert, G. Czjzek, J. Fink, H. Schmidt, *Phys. Lett. A* **1975**, *53*, 31.

[82] S. Sudo, T. Miyadai, *J. Phys. Soc. Jpn.* **1985**, *54*, 3934.

[83] S. Yano, D. Louca, J. Yang, U. Chatterjee, D. E. Bugaris, D. Y. Chung, L. Peng, M. Grayson, M. G. Kanatzidis, *Phys. Rev. B* **2016**, *93*, 024409.

[84] S. Miyasaka, H. Takagi, Y. Sekine, H. Takahashi, N. Mori, R. J. Cava, *J. Phys. Soc. Jpn.* **2000**, *69*, 3166.

[85] I. G. Austin, *Philos. Mag.* **1962**, *7*, 961.

[86] Y. Sekine, H. Takahashi, N. Môri, T. Matsumoto, T. Kosaka, *Physica B: Condens. Matter* **1997**, *237–238*, 148.

[87] C. S. Yoo, B. Maddox, J. H. P. Kiepeis, V. Iota, W. Evans, A. McMahan, M. Y. Hu, P. Chow, M. Somayazulu, D. Husermann, R. T. Scalettar, W. E. Pickett, *Phys. Rev. Lett.* **2005**, *94*, 115502.

[88] H. Oike, K. Miyagawa, H. Taniguchi, K. Kanoda, *Phys. Rev. Lett.* **2015**, *114*, 67002.

[89] V. Guiot, L. Cario, E. Janod, B. Corraze, V. Ta Phuoc, M. Rozenberg, P. Stoliar, T. Cren, D. Roditchev, *Nat. Commun.* **2013**, *4*, 1722.

[90] N. B. Aetukuri, A. X. Gray, M. Drouard, M. Cossale, L. Gao, A. H. Reid, R. Kukreja, H. Ohldag, C. A. Jenkins, E. Arenholz, K. P. Roche, H. A. Dürr, M. G. Samant, S. S. P. Parkin, *Nat. Phys.* **2013**, *9*, 661.

[91] I. I. Mazin, D. I. Khomskii, R. Lengsdorf, J. A. Alonso, W. G. Marshall, R. M. Ibberson, A. Podlesnyak, M. J. Martínez-Lope, M. M. Abd-Elmeguid, *Phys. Rev. Lett.* **2007**, *98*, 176406.

[92] I. A. Nekrasov, G. Keller, D. E. Kondakov, A. V. Kozhevnikov, T. Pruschke, K. Held, D. Vollhardt, V. I. Anisimov, *Phys. Rev. B* **2005**, *72*, 155106.

[93] T. Yoshida, M. Hashimoto, T. Takizawa, A. Fujimori, M. Kubota, K. Ono, H. Eisaki, *Phys. Rev. B* **2010**, *82*, 085119.

[94] C. Kim, C. Kim, W. S. Kyung, S. R. Park, C. S. Leem, D. J. Song, Y. K. Kim, S. K. Choi, W. S. Jung, Y. Y. Koh, H. Y. Choi, Y. Yoshida, R. G. Moore, Z. X. Shen, *J. Phys. Chem. Solids* **2011**, *72*, 556.

[95] J. S. Lee, Y. S. Lee, T. W. Noh, S.-J. Oh, J. Yu, S. Nakatsuji, H. Fukazawa, Y. Maeno, *Phys. Rev. Lett.* **2002**, *89*, 257402.

[96] E. Ko, B. J. Kim, C. Kim, H. J. Choi, *Phys. Rev. Lett.* **2007**, *98*, 226401.

[97] S. Nakatsuji, D. Hall, L. Balicas, Z. Fisk, K. Sugahara, M. Yoshioka, Y. Maeno, *Phys. Rev. Lett.* **2003**, *90*, 137202.

[98] S. Wang, H. Ding, *New J. Phys.* **2005**, *7*, 112.

[99] B. J. Kim, J. Yu, H. Koh, I. Nagai, S. I. Ikeda, S.-J. Oh, C. Kim, *Phys. Rev. Lett.* **2006**, *97*, 106401.

[100] G. van der Laan, J. Zaanen, G. A. Sawatzky, R. Karnatak, J.-M. Esteva, *Phys. Rev. B* **1986**, *33*, 4253.

[101] R. Wang, A. Go, A. J. Millis, *Phys. Rev. B* **2017**, *95*, 045133.

[102] W. Witczak-Krempa, G. Chen, Y. B. Kim, L. Balents, *Annu. Rev. Condens. Matter Phys.* **2014**, *5*, 57.

[103] S. J. Moon, H. Jin, K. W. Kim, W. S. Choi, Y. S. Lee, J. Yu, G. Cao, A. Sumi, H. Funakubo, C. Bernhard, T. W. Noh, *Phys. Rev. Lett.* **2008**, *101*, 226402.

[104] C. H. Kim, H. S. Kim, H. Jeong, H. Jin, J. Yu, *Phys. Rev. Lett.* **2012**, *108*, 106401.

[105] R. Comin, G. Levy, B. Ludbrook, Z. H. Zhu, C. N. Veenstra, J. A. Rosen, Y. Singh, P. Gegenwart, D. Stricker, J. N. Hancock, D. Van Der Marel, I. S. Elfimov, A. Damascelli, *Phys. Rev. Lett.* **2012**, *109*, 266406.

[106] G. Jackeli, G. Khaliullin, *Phys. Rev. Lett.* **2009**, *102*, 017205.

[107] B. Keimer, S. A. Kivelson, M. R. Norman, S. Uchida, J. Zaanen, *Nature* **2014**, *518*, 179.

[108] E. Dagotto, *Science* **2005**, *309*, 257.

[109] C. H. Sohn, M. C. Lee, H. J. Park, K. J. Noh, H. K. Yoo, S. J. Moon, K. W. Kim, T. F. Qi, G. Cao, D. Y. Cho, T. W. Noh, *Phys. Rev. B* **2014**, *90*, 041105.

[110] M. K. Crawford, M. A. Subramanian, R. L. Harlow, J. A. Fernandez-Baca, Z. R. Wang, D. C. Johnston, *Phys. Rev. B* **1994**, *49*, 9198.

[111] H. J. Xiang, M.-H. Whangbo, *Phys. Rev. B* **2007**, *75*, 052407.

[112] D. J. Singh, P. Blaha, K. Schwarz, J. O. Sofo, *Phys. Rev. B* **2002**, *65*, 155109.

[113] D. I. Khomskii, *Basic Aspects of the Quantum Theory of Solids*, Cambridge University Press, Cambridge **2010**.

[114] Y. F. Nie, P. D. C. King, C. H. Kim, M. Uchida, H. I. Wei, B. D. Faeth, J. P. Ruf, J. P. C. Ruff, L. Xie, X. Pan, C. J. Fennie, D. G. Schlom, K. M. Shen, *Phys. Rev. Lett.* **2015**, *114*, 016401.

[115] J. Nichols, J. Terzic, E. G. Bittle, O. B. Korneta, L. E. De Long, J. W. Brill, G. Cao, S. S. A. Seo, *Appl. Phys. Lett.* **2013**, *102*, 141908.

[116] J. Matsuno, K. Ihara, S. Yamamura, H. Wadati, K. Ishii, V. V. Shankar, H. Y. Kee, H. Takagi, *Phys. Rev. Lett.* **2015**, *114*, 247209.

[117] S. Y. Kim, C. H. Kim, L. J. Sandilands, C. H. Sohn, J. Matsuno, H. Takagi, K. W. Kim, Y. S. Lee, S. J. Moon, T. W. Noh, *Phys. Rev. B* **2016**, *94*, 245113.

[118] A. Lupascu, J. P. Clancy, H. Gretarsson, Z. Nie, J. Nichols, J. Terzic, G. Cao, S. S. A. Seo, Z. Islam, M. H. Upton, J. Kim, D. Casa, T. Gog, A. H. Said, V. M. Katukuri, H. Stoll, L. Hozoi, J. Van Den Brink, Y. J. Kim, *Phys. Rev. Lett.* **2014**, *112*, 147201.

[119] K.-H. Kim, H.-S. Kim, M. J. Han, *J. Phys.: Condens. Matter.* **2014**, *26*, 185501.

[120] F. A. Wang, T. Senthil, *Phys. Rev. Lett.* **2011**, *106*, 136402.

[121] H. Watanabe, T. Shirakawa, S. Yunoki, *Phys. Rev. Lett.* **2013**, *110*, 027002.

[122] Z. Y. Meng, Y. B. Kim, H.-Y. Kee, *Phys. Rev. Lett.* **2014**, *113*, 177003.

[123] A. De La Torre, S. McKeown Walker, F. Y. Bruno, S. Ricco, Z. Wang, I. Gutierrez Lezama, G. Scheerer, G. Giriat, D. Jaccard, C. Berthod, T. K. Kim, M. Hoesch, E. C. Hunter, R. S. Perry, A. Tamai, F. Baumberger, *Phys. Rev. Lett.* **2015**, *115*, 176402.

[124] Y. Cao, Q. Wang, J. A. Waugh, T. J. Reber, H. Li, X. Zhou, S. Parham, S.-R. Park, N. C. Plumb, E. Rotenberg, A. Bostwick, J. D. Denlinger, T. Qi, M. A. Hermele, G. Cao, D. S. Dessau, *Nat. Commun.* **2016**, *7*, 11367.

[125] Y. J. Yan, M. Q. Ren, H. C. Xu, B. P. Xie, R. Tao, H. Y. Choi, N. Lee, Y. J. Choi, T. Zhang, D. L. Feng, *Phys. Rev. X* **2015**, *5*, 041018.

[126] I. Battisti, K. M. Bastiaans, V. Fedoseev, A. de la Torre, N. Iliopoulos, A. Tamai, E. C. Hunter, R. S. Perry, J. Zaanen, F. Baumberger, M. P. Allan, *Nat. Phys.* **2016**, *13*, 21.

**ADVANCED
SCIENCE NEWS**

www.advancedsciencenews.com

**ADVANCED
MATERIALS**

www.advmat.de

[127] L. Zhao, D. H. Torchinsky, H. Chu, V. Ivanov, R. Lifshitz, R. Flint, T. Qi, G. Cao, D. Hsieh, *Nat. Phys.* **2016**, *12*, 32.

[128] K. Matsuhira, M. Wakeshima, R. Nakanishi, T. Yamada, A. Nakamura, W. Kawano, S. Takagi, Y. Hinatsu, *J. Phys. Soc. Jpn.* **2007**, *76*, 25.

[129] K. Matsuhira, M. Wakeshima, Y. Hinatsu, S. Takagi, *J. Phys. Soc. Jpn.* **2011**, *80*, 94701.

[130] M. Sakata, T. Kagayama, K. Shimizu, K. Matsuhira, S. Takagi, M. Wakeshima, Y. Hinatsu, *Phys. Rev. B* **2011**, *83*, 041102.

[131] F. F. Tafti, J. J. Ishikawa, A. McCollam, S. Nakatsuji, S. R. Julian, *Phys. Rev. B* **2012**, *85*, 205104.

[132] H. Guo, K. Matsuhira, I. Kawasaki, M. Wakeshima, Y. Hinatsu, I. Watanabe, Z. Xu, *Phys. Rev. B* **2013**, *88*, 060411.

[133] X. Wan, A. M. Turner, A. Vishwanath, S. Y. Savrasov, *Phys. Rev. B* **2011**, *83*, 205101.

[134] K. Ueda, J. Fujioka, Y. Takahashi, T. Suzuki, S. Ishiwata, Y. Taguchi, Y. Tokura, *Phys. Rev. Lett.* **2012**, *109*, 136402.

[135] L. Savary, E.-G. Moon, L. Balents, *Phys. Rev. X* **2014**, *4*, 041027.

[136] D. Mandrus, J. R. Thompson, R. Gaal, L. Forro, J. C. Bryan, B. C. Chakoumakos, L. M. Woods, B. C. Sales, R. S. Fishman, V. Keppens, *Phys. Rev. B* **2001**, *63*, 195104.

[137] J. Yamaura, K. Ohgushi, H. Ohsumi, T. Hasegawa, I. Yamauchi, K. Sugimoto, S. Takeshita, A. Tokuda, M. Takata, M. Udagawa, M. Takigawa, H. Harima, T. Arima, Z. Hiroi, *Phys. Rev. Lett.* **2012**, *108*, 247205.

[138] W. J. Padilla, D. Mandrus, D. N. Basov, *Phys. Rev. B* **2002**, *66*, 035120.

[139] S. Tardif, S. Takeshita, H. Ohsumi, J. Yamaura, D. Okuyama, Z. Hiroi, M. Takata, T. Arima, *Phys. Rev. Lett.* **2015**, *114*, 147205.

[140] H. Shinaoka, T. Miyake, S. Ishibashi, *Phys. Rev. Lett.* **2012**, *108*, 247204.

[141] G.-W. Chern, C. D. Batista, *Phys. Rev. Lett.* **2011**, *107*, 186403.

[142] N. T. Vandenexorre, E. H. H. Brusset, *Spectrochim. Acta* **1981**, *37*, 113.

[143] C. Felser, B. Yan, *Nat. Mater.* **2016**, *15*, 1149.

[144] S. Lee, J.-G. Park, D. T. Adroja, D. Khomskii, S. Streltsov, K. A. McEwen, H. Sakai, K. Yoshimura, V. I. Anisimov, D. Mori, R. Kanno, R. Ibberson, *Nat. Mater.* **2006**, *5*, 471.

[145] F. D. M. Haldane, *Phys. Lett. A* **1983**, *93*, 464.

[146] F. D. M. Haldane, *Phys. Rev. Lett.* **1983**, *50*, 1153.

[147] P. Fazekas, E. Tosatti, *Physica B+C* **1980**, *99*, 183.

[148] L. Stojchevska, I. Vaskivskyi, T. Mertelj, P. Kusar, D. Svetin, S. Brazovskii, D. Mihailovic, *Science* **2014**, *344*, 177.

[149] M. Kratochvilova, A. D. Hillier, A. R. Wildes, L. Wang, S.-W. Cheong, J-G. Park, *npj Quantum Mater.* **2017**, *2*, 42.

[150] T. Ishiguro, H. Sato, *Phys. Rev. B* **1991**, *44*, 2046.

[151] M. Bovet, S. Van Smaalen, H. Berger, R. Gaal, L. Forró, L. Schlapbach, P. Aebi, *Phys. Rev. B* **2003**, *67*, 125105.

[152] L. Ma, C. Ye, Y. Yu, X. F. Lu, X. Niu, S. Kim, D. Feng, D. Tománek, Y.-W. Son, X. H. Chen, Y. Zhang, *Nat. Commun.* **2016**, *7*, 10956.

[153] P. Darancet, A. J. Millis, C. A. Marianetti, *Phys. Rev. B* **2014**, *90*, 045134.

[154] Y. Miura, Y. Yasui, M. Sato, N. Igawa, K. Kakurai, *J. Phys. Soc. Jpn.* **2007**, *76*, 33705.

[155] J. Park, T.-Y. Tan, D. T. Adroja, A. Daoud-Aladine, S. Choi, D.-Y. Cho, S.-H. Lee, J. Kim, H. Sim, T. Morioka, H. Nojiri, V. V Krishnamurthy, P. Manuel, M. R. Lees, S. V Streltsov, D. I. Khomskii, J.-G. Park, *Sci. Rep.* **2016**, *6*, 25238.

[156] S. A. J. Kimber, I. I. Mazin, J. Shen, H. O. Jeschke, S. V. Streltsov, D. N. Argyriou, R. Valentí, D. I. Khomskii, *Phys. Rev. B* **2014**, *89*, 081408.

[157] D. I. Khomskii, *Phys. Scr.* **2005**, *72*, CC8.

[158] G. Jackeli, D. I. Khomskii, *Phys. Rev. Lett.* **2008**, *100*, 147203.

[159] A. Pergament, A. Crunteanu, A. Beaumont, arXiv:1601.06246, **2015**.

[160] Z. Yang, C. Ko, S. Ramanathan, *Annu. Rev. Mater. Res.* **2011**, *41*, 337.

[161] Y. Zhou, S. Ramanathan, *Proc. IEEE* **2015**, *103*, 1289.

[162] Y. Zhou, S. Ramanathan, *Crit. Rev. Solid State Mater. Sci.* **2013**, *38*, 286.

[163] F. Chudnovskiy, S. Luryi, B. Spivak, in *Future Trends in Microelectronics: The Nano Millennium*, Wiley, New York **2002**, pp. 148–155.

[164] E. Janod, J. Tranchant, B. Corraze, M. Querré, P. Stoliar, M. Rozenberg, T. Cren, D. Roditchev, V. T. Phuoc, M.-P. Besland, L. Cario, *Adv. Funct. Mater.* **2015**, *25*, 6287.

[165] P. Stoliar, L. Cario, E. Janod, B. Corraze, C. Guillot-Deudon, S. Salmon-Bourmand, V. Guiot, J. Tranchant, M. Rozenberg, *Adv. Mater.* **2013**, *25*, 3222.

[166] E. Y. Ma, Y.-T. Cui, K. Ueda, S. Tang, K. Chen, N. Tamura, P. M. Wu, J. Fujioka, Y. Tokura, Z.-X. Shen, *Science* **2015**, *350*, 538.

[167] H. T. Hirose, J. I. Yamaura, Z. Hiroi, *Sci. Rep.* **2017**, *7*, 42440.

[168] S. S. P. Parkin, M. Hayashi, L. Thomas, *Science* **2008**, *320*, 190.

[169] A. Agrawal, A. Choudhary, *APL Mater.* **2016**, *4*, 053208.

[170] Y. Liu, T. Zhao, W. Ju, S. Shi, S. Shi, S. Shi, *J. Mater.* **2017**, *3*, 159.

[171] J. B. Torrance, P. Lacorre, A. I. Nazzal, E. J. Ansaldo, C. Niedermayer, *Phys. Rev. B* **1992**, *45*, 8209.

[172] P.-H. Xiang, N. Zhong, C.-G. Duan, X. D. Tang, Z. G. Hu, P. X. Yang, Z. Q. Zhu, J. H. Chu, *J. Appl. Phys.* **2013**, *114*, 243713.

[173] A. Tiwari, C. Jin, J. Narayan, *Appl. Phys. Lett.* **2002**, *80*, 4039.

[174] Y. Zhou, X. Guan, H. Zhou, K. Ramadoss, S. Adam, H. Liu, S. Lee, J. Shi, M. Tsuchiya, D. D. Fong, S. Ramanathan, *Nature* **2016**, *534*, 231.

[175] J. Shi, Y. Zhou, S. Ramanathan, *Nat. Commun.* **2014**, *5*, 4860.

[176] H. Y. Hwang, S. W. Cheong, P. G. Radaelli, M. Marezio, B. Batlogg, *Phys. Rev. Lett.* **1995**, *75*, 914.

[177] O. Friedt, M. Braden, G. André, P. Adelmann, S. Nakatsuji, Y. Maeno, *Phys. Rev. B* **2001**, *63*, 174432.

[178] F. Nakamura, M. Sakaki, Y. Yamanaka, S. Tamaru, T. Suzuki, Y. Maeno, *Sci. Rep.* **2013**, *3*, 02536.

[179] R. V. Yusupov, D. Mihailovic, C. V. Colin, G. R. Blake, T. T. M. Palstra, *Phys. Rev. B* **2010**, *81*, 075103.

[180] J. Orenstein, *Phys. Today* **2012**, *65*, 44.

[181] C. Giannetti, M. Capone, D. Fausti, M. Fabrizio, F. Parmigiani, D. Mihailovic, *Adv. Phys.* **2016**, *65*, 58.

[182] A. Cavalleri, C. Tóth, C. W. Siders, J. A. Squier, F. Ráksi, P. Forget, J. C. Kieffer, *Phys. Rev. Lett.* **2001**, *87*, 237401.

[183] A. Cavalleri, T. Dekorsy, H. H. W. Chong, J. C. Kieffer, R. W. Schoenlein, *Phys. Rev. B* **2004**, *70*, 161102.

[184] M. K. Liu, B. Pardo, J. Zhang, M. M. Qazilbash, S. J. Yun, Z. Fei, J. H. Shin, H. T. Kim, D. N. Basov, R. D. Averitt, *Phys. Rev. Lett.* **2011**, *107*, 066403.

[185] M. Rini, R. Tobey, N. Dean, J. Itatani, Y. Tomioka, Y. Tokura, R. W. Schoenlein, A. Cavalleri, *Nature* **2007**, *449*, 72.

[186] N. Takubo, Y. Ogimoto, M. Nakamura, H. Tamaru, M. Izumi, K. Miyano, *Phys. Rev. Lett.* **2005**, *95*, 017404.

[187] S. Y. Kim, H. Yoon, C. H. Sohn, J. Son, S. Chang, J. Son, S. J. Moon, B. C. Park, T. W. Noh, unpublished.

[188] Y. J. Yu, Y. Xu, L. P. He, M. Kratochvilova, Y. Y. Huang, J. M. Ni, L. Wang, S.-W. Cheong, J.-G. Park, S. Y. Li, *Phys. Rev. B* **2017**, *96*, 081111(R).

[189] E. Arcangeletti, L. Baldassarre, D. Di Castro, S. Lupi, L. Malavasi, C. Marini, A. Perucchi, P. Postorino, *Phys. Rev. Lett.* **2007**, *98*, 196406.

[190] Y. Zhou, X. Chen, C. Ko, Z. Yang, C. Mouli, S. Ramanathan, *IEEE Electron Device Lett.* **2013**, *34*, 220.

[191] H. Yoon, M. Choi, T.-W. Lim, H. Kwon, K. Ihm, J. K. Kim, S.-Y. Choi, J. Son, *Nat. Mater.* **2016**, *15*, 1113.

[192] V. Y. Zerov, Y. V. Kulikov, V. N. Leonov, V. G. Malyarov, I. a. Khrebtov, I. I. Shaganov, *J. Opt. Technol.* **1999**, *66*, 387.

[193] Z. Topalian, S. Li, G. A. Niklasson, C. G. Granqvist, *J. Appl. Phys.* **2015**, *117*, 025303.

[194] S. Friedemann, H. Chang, M. B. Gamża, P. Reiss, X. Chen, P. Alireza, W. A. Coniglio, D. Graf, S. Tozer, F. M. Grosche, *Sci. Rep.* **2016**, *6*, 25335.

[195] A. Husmann, D. S. Jin, Y. V. Zastavker, T. F. Rosenbaum, X. Yao, J. M. Honig, *Science* **1996**, *274*, 1874.

[196] D. Fobes, E. Vehstedt, J. Peng, G. C. Wang, T. J. Liu, Z. Q. Mao, *J. Appl. Phys.* **2012**, *111*, 83709.

[197] S. Nakatsuji, S. I. Ikeda, Y. Maeno, *J. Phys. Soc. Jpn.* **1997**, *66*, 1868.

[198] C. Alexander, G. Cao, V. Dobrosavljevic, S. McCall, J. Crow, E. Lochner, R. Guertin, *Phys. Rev. B* **1999**, *60*, R8422.

[199] R. Ishikawa, H. Taniguchi, S. Kuan Goh, S. Yonezawa, F. Nakamura, Y. Maeno, *J. Phys. Conf. Ser.* **2012**, *400*, 22036.

[200] M. Braden, G. André, S. Nakatsuji, Y. Maeno, *Phys. Rev. B* **1998**, *58*, 847.

[201] W. Yang, Y. Xie, W. Zhu, K. Park, A. Chen, Y. Losovyj, Z. Li, H. Liu, M. Starr, J. A. Acosta, C. Tao, N. Li, Q. Jia, J. J. Heremans, S. Zhang, *Sci. Rep.* **2016**, *7*, 7740.

1704777  (20 of 20)